Effect of Hadronic Phase Lifetime on Identified Particle Production and Elliptic Flow in Heavy-Ion Collisions

A THESIS

Submitted in partial fulfillment of the

requirements for the award of the degree

of

Master of Science

by

Vikas Yadav

under the guidance of

Prof. Raghunath Sahoo

DISCIPLINE OF PHYSICS

INDIAN INSTITUTE OF TECHNOLOGY INDORE

June 2020

INDIAN INSTITUTE OF TECHNOLOGY INDORE

CANDIDATE'S DECLARATION

I hereby certify that the work which is being presented in the thesis entitled "**Effect of Hadronic Phase Lifetime on Identified Particle Production and Elliptic Flow in Heavy-Ion Collisions"** in the partial fulfillment of the requirements for the award of the degree of **MASTER OF SCIENCE** and submitted in the **DISCIPLINE OF PHYSICS, Indian Institute of Technology Indore**, is an authentic record of my own work carried out during the time period from July 2019 to June 2020 under the supervision of Prof. Raghunath Sahoo, Associate Professor, Discipline of Physics, Indian Institute of Technology Indore , Indore, M.P., India.

The matter presented in this thesis has not been submitted by me for the award of any other degree of this or any other institute.

Vikas Yadav
18/6/20

(VIKAS YADAV)

This is to certify that the above statement made by the candidate is correct to the best of my knowledge.

M.Sc. Thesis Supervisor

(Prof. RAGHUNATH SAHOO)

VikasYadav has successfully given his M.Sc. Oral Examination held on 24.06.2020.

M.Sc. Thesis Supervisor
Date: 07.07.2020

Convener, DPGC
Date: 07.07.2020

PSPC Member 1
Date: 07.07.2020
(Dr. M. Mahato)

PSPC Member 2
Date: 07.07.2020
(Dr. S. Vasudevan)

Dedicated

to

My Family

ACKNOWLEDGEMENT

I would like to express my deepest gratitude to my supervisor Prof. Raghunath Sahoo for allowing me to work in the exciting field of "Relativistic heavy-ion Collisions". He has been a constant source of inspiration to me for pursuing experimental high energy physics. His guidance, fundamental approach to research, insights in experimental work, and rigorous discussions have been of great help for me to have a clear understanding of the project. Without him, this project would not have been possible. I would also like to thank my PSPC committee members, Dr. Manavendra Mahato, and Dr. Srivathsan Vasudevan for their advice.

I would like to thank Rutuparna didi, for guiding me to learn AMPT model and coding ROOT macros for generating events using AMPT model and analysing the data.

I would like to thank all my friends for their support and making the stay at IIT Indore a memorable one. I would also like to thank Suman bhaiya, Golam bhaiya, Dhananjaya bhaiya and all labmates for their continuous support.

Vikas Yadav

ABSTRACT

This thesis presents the study of elliptic flow (v_2) created in heavy-ion collisions. After getting a detailed idea about elliptic flow, a simulation of the collision of heavy nuclei (Xe+Xe) at $\sqrt{s_{NN}} = 5.44$ TeV for 10 thousand events using the AMPT-SM model is done. The simulated data are analysed to obtain the p_{T} spectra and elliptic flow (v_2) of identified charged particles.

In this work, transverse momentum spectra (p_{T}) are plotted for identified particles such as π, K, $\mathrm{K_s^0}$, p, ϕ, and Λ in different centralities. Comparison of the p_{T}-spectra shows that the differential yield of particles decreases with an increase in transverse momentum p_{T}. Finally, the "Elliptic flow" (v_2) of identified particles is studied, which is a very important property for momentum anisotropies produced in the collective flow of the particle. The plot of v_2 as a function of transverse momentum (p_{T}) for different centrality is obtained. The non-zero value of v_2 confirms the presence of anisotropy in the collective flow of identified particles. The elliptic flow of proton (baryon) is compared with a phi (meson), which is comparable in mass with different quark content. v_2 vs p_{T} is plotted for different centralities. v_2 vs p_{T} is plotted for different hadronic cascade time, τ_{HC}, which show that v_2 increases with an increase in τ_{HC}. The plot of average elliptic flow ($< v_2 >$) of the charged particle as a function of centrality shows that it increases gradually up to mid-central collisions and then starts decreasing for the peripheral collisions.

Contents

List of Figures

Chapter 1

Introduction

The basic building blocks of the Universe are fundamental particles which are governed by four fundamental forces. Such forces are electromagnetic force, weak force, strong force, and gravity, which are mediated by the photons, W and Z gauge bosons, gluons and gravitons respectively. The photon and the gluons are massless, while the W and Z bosons are very massive. The standard model of particle physics explains the relation between these particles and the four fundamental forces. The fundamental theory of strong interactions is known as Quantum Chromodynamics (QCD). QCD predicts that at high energy density/at high temperature, the hadronic matter will turn into a plasma of deconfined quarks and gluons (QGP). The lattice Quantum Chromodynamics calculation predicts that a phase transition can occur from hadronic matter to a gas of deconfined quarks and gluons. This phase transition occurs at a high temperature called critical temperature (T_c), which is approximately equal to 160 MeV [1].

In few microseconds, just after the Big-Bang, the Universe was filled with very hot and dense matter consisting of the fundamental particles called quarks and gluons. This scenario can be created in the laboratory by colliding heavy-nuclei and possibly by hadronic collisions at the GeV/TeV energies at the RHIC/LHC.

1.1 QCD phase diagram

Quantum Chromodynamics (QCD) is the theory of strong interaction. Its elementary particles are the quarks and gluons, which are confined inside hadrons at low energy due to the infrared slavery property of the QCD. Whereas, another property namely asymptotic freedom in the QCD leads to a deconfined state called the QGP phase through a phase transition at sufficiently higher energies. The phase transition of the QCD matter is controlled by the temperature (T) and net baryo-chemical potential (μ_B) as shown in Fig. 1.1. To trigger deconfinement, we have to increase the temperature or the baryo-chemical potential or both which can be achieved in the experiment by varying the collision energy of the ultra-relativistic nuclei. The Large Hadron Collider (LHC) works in the regime of high

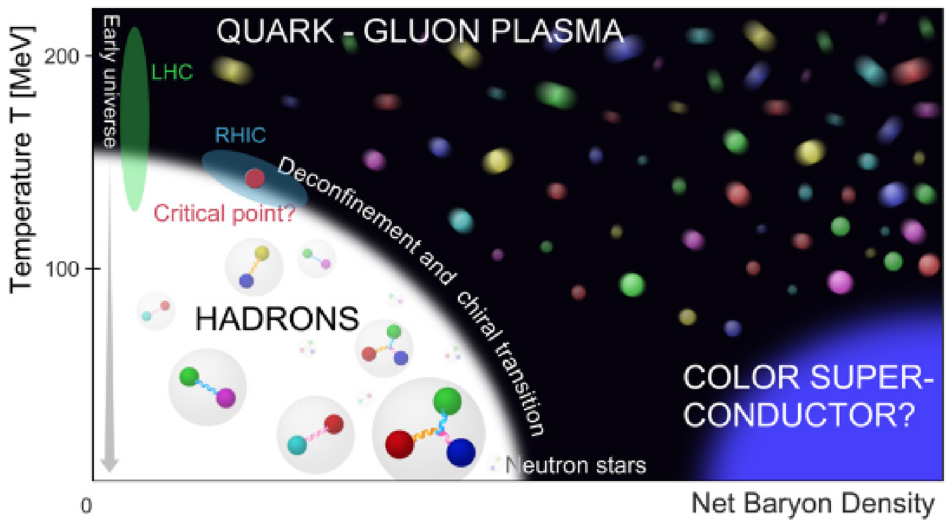

Figure 1.1: (Color online) QCD phase Diagram

temperature and extremely low baryo-chemical potential which was the scenario after a few microseconds of the Big Bang. In contrary, the deconfined QCD matter can also be observed with high baryo-chemical potential and low temperature which is believed to exist in the core of neutron stars. Lattice QCD (lQCD) predicts that the transition to a QGP phase at a critical temperature, T_c in the order of 140–170 MeV which corresponds to the critical energy density, $\epsilon_c \simeq 1\ GeV/fm^3$ [1]. The phase transition from hadronic degrees of freedom to partonic one is a cross-over at high temperature and zero baryo-chemical potential as predicted by lQCD. Many phenomenological models predict a first-order phase transition at finite μ_B. Therefore, the QCD phase diagram features a critical point where the first-order phase transition ends.

1.2 Relativistic heavy-ion Collisions

The purpose of heavy-ion collisions is to study the properties of matter at high energies. In such collisions, the energy density is very high due to a large amount of energy deposition over a small region for a very short time period. The high energy density produced in the collision may give rise to new forms of matter such as the quark-gluons plasma (QGP). In a relativistic heavy-ion collision, the center of mass-energy is the energy available to produce new particles. In these collisions, the produced particle multiplicities are very high which means that the number of particles produced in the collision is much greater than the initial number of nucleons. The particles produced in the collision can be treated as a large macroscopic system, hence theories such as thermodynamics, hydrodynamics, and field theory at finite temperature and density can be used to describe the system.

1.3 Evolution of a heavy-ion collision

The system formed in relativistic heavy-ion collisions and its evolution, can be studied through the space-time evolution of the heavy-ion collisions. As shown in the Fig. 1.2, the different stages of the space-time evolution of the collisions can be described by the Bjorken scenario and discussed in details as follows [2]:

- **Pre-equilibrium stage:**

  This is the stage just after the collisions where the multiple interactions occur among the partons. The energy density is maximum just at the moment of collision and the produced system is far from equilibrium. Finally, the multiple scattering between the partons leads

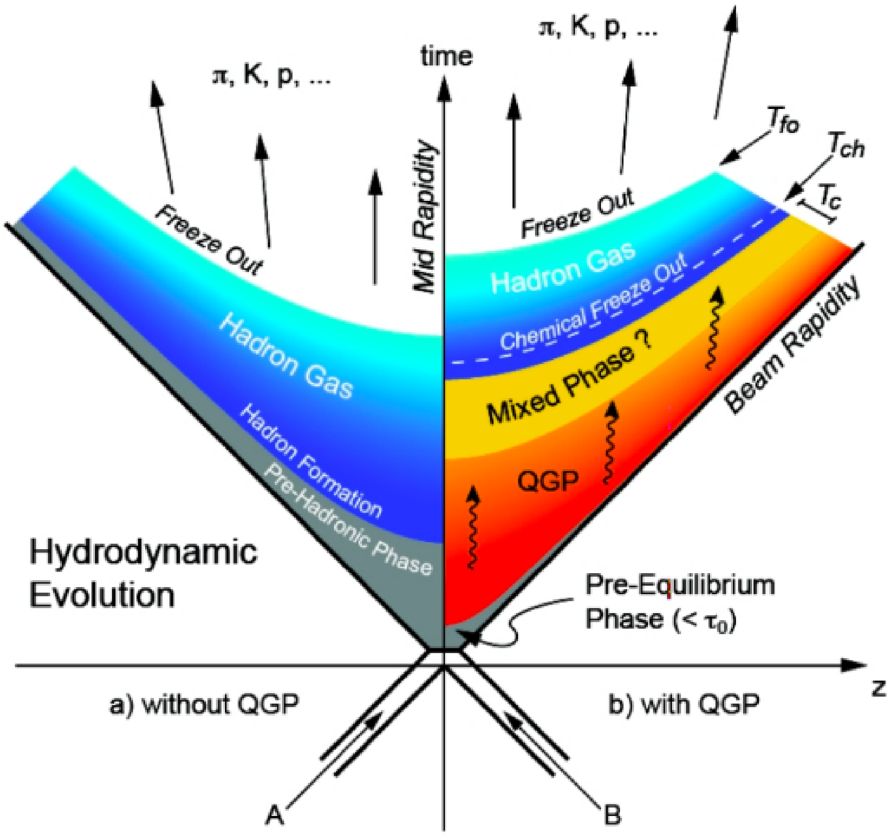

Figure 1.2: (Color online) The space-time evolution of heavy-ion collisions.

the system towards thermalization.

- **QGP formation and hydrodynamic expansion:**

  If the energy density is above the critical energy density of the QCD phase transition (≈1 GeV/fm^3), then we expect a phase transition from the hadronic degrees of freedom to the partonic one. At the beginning of heavy-ion collisions, the presence of a higher amount of gluons with respect to the quarks is often considered as a gluon plasma (Glasma). Due to the generation of thermal pressure gradients, the QGP gradually expands and cools down very quickly, and the partons inside the fireball re-scatter elastically and inelastically.

- **Mixed stage:**

  The system produced in the high energy collisions gets cooler with the expansion and the energy density decreases, which leads to the hadronization of the produced quarks and the gluons. There are two different mechanisms of hadronization: (1) Fragmentation and (2) Coalescence. In string fragmentation, the produced partons are recombined with their parent strings and converts to hadrons. Whereas in the string-melting, the partons start converting into hadrons when they stop interacting with each other.

- **Chemical freeze-out (CFO):**

  In this phase, the inelastic collisions between the hadrons stop and the formation of new particle ceases. Hence, hadron abundances remain fixed during the system evolution after the chemical freeze-out. However, due to elastic collisions, the local equilibrium is still maintained and the system cools down and evolves with a fixed number of hadrons.

- **Kinetic freeze-out (KFO):**

  After the CFO phase, the final state particles still undergo elastic scattering by altering the transverse momentum until the mean free path of the hadrons exceeds the system size. Finally, we get a stream of hadrons in the final state and this is called kinetic freeze-out.

The whole system which forms QGP to free streaming particles is called the fireball. The phase between kinetic freeze-out and chemical freeze-out is called as the hadronic phase.

1.4 Kinematics variables

According to the special theory of relativity, the speed of light (c) is constant in all inertial frames of reference, which is known as invariance of speed of light. In heavy-ion collisions, physical observables such as position and four momenta are treated relativistically. So, it is convenient to use kinematics variables which take simple form under Lorentz transformation for the change of frame of reference [3]. A few of them are the rapidity, pseudorapidity and invariant yield, etc.

1.4.1 Transverse momentum and transverse mass

In ultra-relativistic heavy-ion collisions, two Lorentz contracted nuclei approach each other with velocities nearly equal to the speed of light. Usually, the z-axis is defined as the beam axis and the plane perpendicular to the beam axis is known as the transverse plane. The particle momentum in the transverse plane is known as the transverse momentum (p_{T}) and is defined as:

$$p_T = \sqrt{p^2 - p_z^2} \tag{1.1}$$

In heavy-ion collisions, the transverse momentum of the final state particle is one of the important physical observable. The high p_{T} particles mostly arise from the hard partonic collisions whereas soft partonic collisions give rise to low p_{T} particles. The transverse mass (m_T) of a particle contains both mass and momentum in the transverse plane and this quantity is invariant under the Lorentz boost (relative motion with a constant velocity). The transverse mass (m_T) is defined as:

$$m_T = \sqrt{m^2 + p_T^2} \tag{1.2}$$

where m and p_{T} are the mass and the transverse momentum of the particle respectively.

1.4.2 Rapidity and pseudorapidity

The velocity is not an additive quantity in Lorentz transformation. i.e. non-linear in successive transformation. So, an alternative to velocity, the rapidity is frequently used in the ultra-relativistic collisions. In terms of energy-momentum components p_0 and p_z the rapidity of a particle can be written as:

$$y = \frac{1}{2} \ln \left(\frac{p_0 + p_z}{p_0 - p_z} \right) \tag{1.3}$$

This is a dimensionless quantity related to the ratio of the forward light-cone momentum (p_+) to the backward light-cone momentum (p_-). It can be both either positive or negative. In a non-relativistic case, the rapidity of a particle is equal to the velocity of the particle in the units of speed of light (c). For the estimation of the rapidity of a particle, both the energy (E) and the total momentum (p) are needed. In the experiment, it is difficult to measure both the energy (E) and the total momentum (p) precisely. However, to avoid this problem the pseudorapidity (η) can be used which depends only on the angle (θ) between the three-momentum vector of the particle and the beam axis. The pseudorapidity is defined as:

$$\eta = -\ln \left(\tan \frac{\theta}{2} \right) \tag{1.4}$$

For highly relativistic particle, the p_{T} of a particle is much larger compared to its mass and the rapidity converges to the definition of pseudorapidity, thus y $\approx \eta$ [4].

1.5 Signatures of QGP

The formation of QGP in the heavy-ion collisions cannot be observed directly. Extremely hot matter formed in such collisions undergo space-time evolution which cools down and the quarks get hadronized. However, when the elastic and inelastic processes cease, a spray of stable particles get detected by the detectors. From these final state particles, the information should be extracted about the space-time evolution of the collision. It appears that there is no single unique signal which can unambiguously prove the formation of QGP in the evolution of a heavy-ion collision. So, there are several signatures which can indicate the presence of the QGP and a few of these signatures are given below.

- **J/ψ suppression:** The presence of the color charges in the QGP suppresses the formation of the bound state of the charm (c)-anticharm ($\bar{c}$) pair due to the color screening effect and thus the formation of J/ψ meson. This is similar to Debye screening in electrostatics.

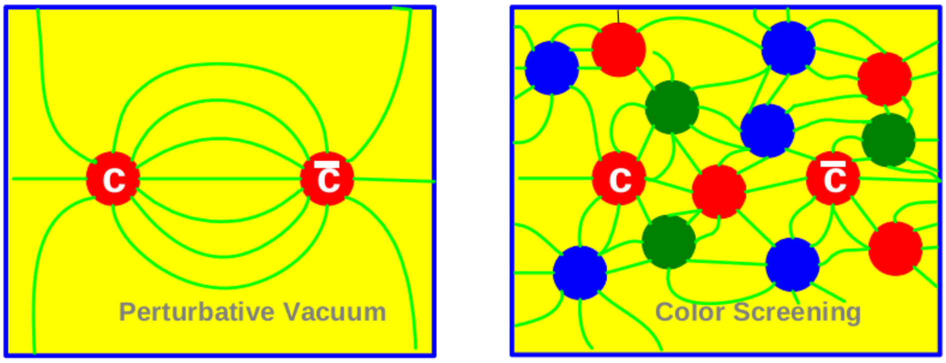

Figure 1.3: (Color online) A description of J/ψ suppression. In the left panel the J/ψ quark-antiquark pair is held together by the strong force but in the right panel the quark and antiquark pair is shielded by the other quarks and the binding is broken.

  A pictorial representation of this is shown in Fig. 1.3. The quark-antiquark pair bound together by the strong force, however, when they are in plasma of many other quarks and antiquarks of different colors they are unable to remain bound together and therefore the number of J/ψ is suppressed.

- **Jet quenching:**

  The double peak structure in the relativistic heavy-ion collisions can be understood in terms of two jet events. However, in the heavy-ion collisions, the away side peak is strongly suppressed which is the experimental evidence of jet quenching.

  As shown in the Fig. 2.2, in case a di-jet is produced near the surface of fireball (QGP), one of the jets escapes into the vacuum and fragments. The other enters the medium and loses its energy and momentum in the medium before fragmentation.

- **Strangeness enhancement:**

  In high-multiplicity pp-collisions, strange quark pairs (s$\bar{s}$) can be formed from the available kinetic energy [5]. Strange quarks are not

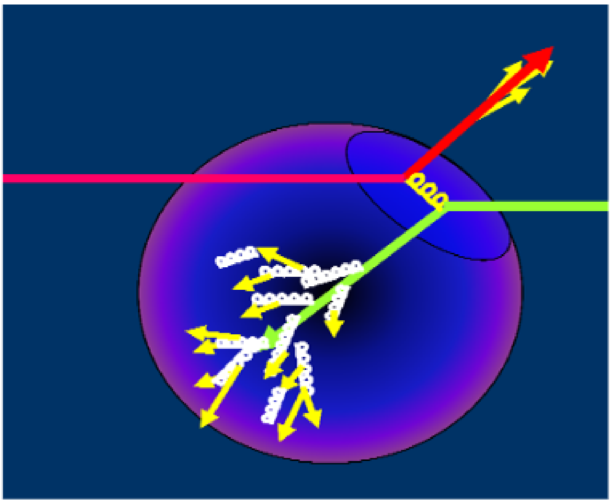

Figure 1.4: (Color online) A descriptive example of jet suppression. The near side jet in red is detected while the far side jet in green is lost inside the dense QGP medium.

present in the protons before the collision. The probability to form a strange quark pair is small and therefore the number of strange hadrons are formed when the s and $\bar{s}$ pair with other quarks. In a nucleus-nucleus collision, the probability to form $s\bar{s}$ is larger as the QGP medium is most probably formed in such a collision, where the probability is expected to increase even more with the centrality. An enhancement in the number of strange particle production in high energy collisions with centrality and collision energy is a signature of the presence of the QGP.

- **Collective flow:**

  The azimuthal momentum distribution of the final state particles in the heavy-ion collisions may reveal the properties of the produced medium. If the system is in thermal equilibrium, the resulting pressure gradient generates a common velocity in the outgoing particles, which is known as collective flow. This includes a common radial expansion affecting the thermal spectra of outgoing particles and an anisotropic expansion which affects the spatial orientation of particle momenta. The first component is called directed flow (v_1) whereas, the second term corresponds to anisotropic flow. The most dominant contribution to anisotropic flow comes from the elliptic flow (v_2). Collective flow is sensitive to the equation of state of the hydrodynamically expanding system.

Chapter 2

Event Simulation and Elliptic Flow using AMPT

In this work, we have used A Multiphase Transport Model (AMPT) to generate events in Xe+Xe collisions at $\sqrt{s_{NN}} = 5.44$ TeV. Here, we have introduced non-zero deformities to the Xe nuclei to have a similar environment as in experiments. More technical details are given below:

2.1 Simulation techniques

This chapter focuses on data generation methodology and its analysis to interpret the results. Our analysis involves the following steps such as:

- Event (data) generations
- Storing data in Tree file
- Analysis of data for meaningful physics results

To perform the above analysis, we have used AMPT for the event generation and ROOT for the analysis of the generated data.

2.2 A Multi-Phase Transport (AMPT) model

2.2.1 Structure of AMPT

A Multi-Phase Transport (AMPT) model (Fig. 2.1) consists of four main components: (1) the initial conditions, (2) partonic interactions, (3) conversion from the partonic to the hadronic matter, and (4) the hadronic interactions [6]. For each component different models are used as follows:

1. Initial Conditions: The initial conditions, which include the spatial and momentum distributions of minijet partons and soft string excitations are obtained from the Heavy Ion Jet Interaction Generator (HIJING) model.

2. Partonic Interactions: Scatterings among partons are modeled by Zhangs Parton Cascade (ZPC), which at present includes only two-body scatterings with cross-sections that are obtained from the pQCD with screening masses.

3. Partonic to Hadronic conversion: In the default AMPT model, the hadronization of the produced partons are recombined with their parent strings when they stop interacting, and the resulting strings are converted to hadrons using the Lund string fragmentation model. In the AMPT model with string melting, a quark coalescence model is used instead to combine partons into hadrons.

4. Hadronic interactions: Scatterings among the resulting hadrons are described by A Relativistic Transport (ART) model.

Final results from the AMPT model are obtained after the hadronic interactions are terminated at a cutoff time (t_{cut}) when observables under study are considered to be stable. For our study, we have used the AMPT string melting version (AMPT-SM).

2.2.2 Versions of AMPT: Default and String Melting

Based on the two models used for the third stage that is partonic matter to the hadronic matter conversion stage, two variants of the AMPT model are classified as:

(i) Default model.
In the Default AMPT model, Partons are recombined with their parent strings when they stop interacting, and the resulting strings are converted to hadrons using the Lund string fragmentation model.

(ii) String Melting (SM) model.
In the AMPT model with string melting, a quark coalescence model is used to combine partons into hadrons. We have chosen the AMPT (SM) for our study.

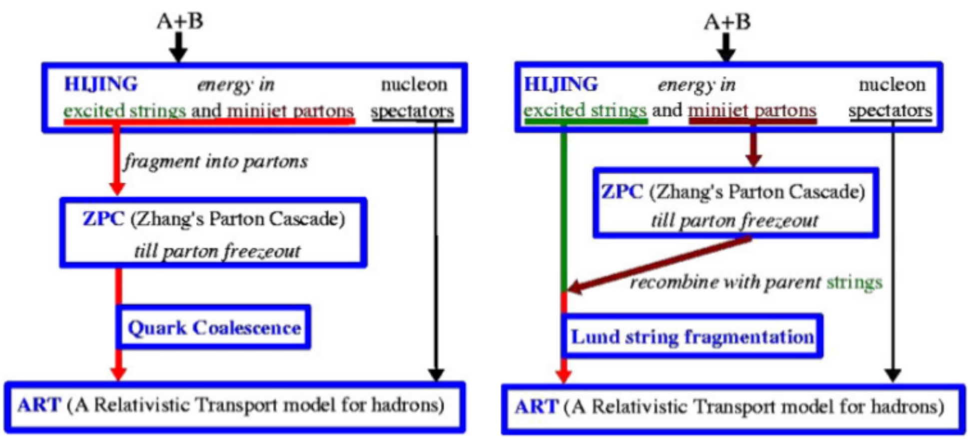

Figure 2.1: (Color online) Structure of the default and string-melting model.

2.2.3 Implementation of deformation in AMPT

For deformed nucleus such as Xe, we may include deformation parameter (β_n), along with spherical harmonics ($Y_{nl}(\theta)$), in the Woods-Saxon (WS) function. This is known as the modified Woods-Saxon (MWS) density distribution. We have used MWS within the HIJING model to calculate initial distributions of partons for random configuration in the collisions of Xe nuclei. Let us now describe briefly the MWS:

Nucleon density in HIJING is usually written as a three parameter Fermi distribution as written below:

$$\rho(r) = \rho_0[\frac{1 + w(r/R)^2}{1 + exp[(r - R)/a]}]\,. \tag{2.1}$$

Here ρ_0 is the nuclear matter density in the center of the nucleus, R is the radius of the nucleus from its center. The parameter, a, is the skin depth or surface thickness, r is a position parameter and distance of any point from the center of the nucleus, and w is the deviation from a smooth spherical surface. Au^{197} or Pb^{208} nucleus is assumed here to have a uniform distribution of nucleons in its approximately spherical volume and smooth surface so that w can be taken to be zero. This reduces eqn. 2.1 to Woods-Saxon distribution, which has been used in HIJING in most cases. Now, the modified Woods-Saxon function is written as:

$$\rho(r) = \frac{\rho_0}{1 + exp[(r - R)/a]}\,. \tag{2.2}$$

When we use an axially symmetric or prolate deformed nucleus (viz. U^{238}, Xe^{56}, etc.), nuclear radius (R), has been modified to include spherical harmonics. The modified Woods-Saxon nuclear radius may be written as:

$$R_{A\Theta} = R[1 + \beta_2 Y_{20}(\theta) + \beta_4 Y_{40}(\theta)], \tag{2.3}$$

where the symbols β_i are deformation parameters. In case of Xe nucleus, we have used deformation parameters, $\beta_2 = 0.162$ and $\beta_4 =$ -0.003. The spherical harmonics (Y_{20}), and (Y_{40}) are given as:

$$
\begin{aligned}
Y_{20}(\theta) &= \frac{1}{4}\sqrt{\frac{5}{\pi}}(3\ cos^2\theta - 1) \\
Y_{40}(\theta) &= \frac{3}{16\sqrt{\pi}}(35\ cos^4\theta - 30\ cos^2\theta + 3)\,. \qquad (2.4)
\end{aligned}
$$

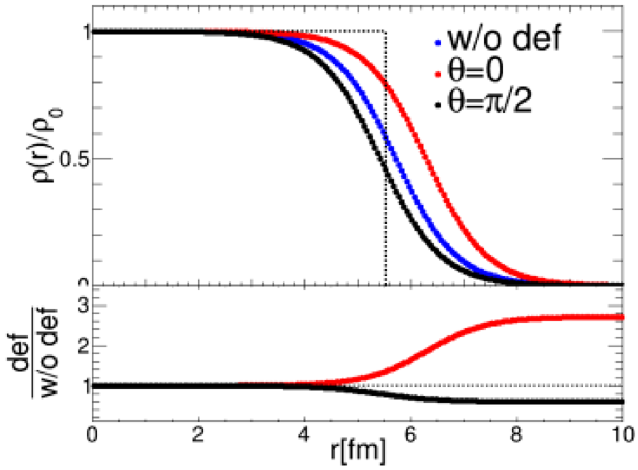

Figure 2.2: (Color online) The nuclear density profile for Xe nucleus [7].

Using deformation parameters β_n and spherical harmonics $Y_{nl}(\theta)$, the deformed radius ($R_{A\theta}$) for Xe nucleus, when $\theta = 0$, $\frac{\pi}{2}$ and π are found out to be 6.074 fm, 5.24 fm and 6.074 fm respectively [7].

Hadronic phase time (τ_{HC}) is used as one of the inputs for colliding nuclei in the AMPT [8]. The termination time of the hadronic cascade can be tuned by an input parameter called NTMAX, which is the number of time steps (each step corresponds to 0.2 fm) of the hadronic interactions. The default value of NTMAX is 150 which corresponds to a value of τ_{HC} = 30 fm. We are generating the AMPT data for τ_{HC} = 5 fm, 10 fm, 15 fm, 20 fm and 25 fm to study the hadronic phase time dependence on the observables such as transverse momentum spectra and elliptic flow of identified charged particles.

2.3 ROOT analysis

ROOT is a framework for data processing, born at CERN, at the heart of the research on high-energy physics. Every day, thousands of physicists use ROOT applications to analyze their data or to perform simulations. It is an open-source project coordinated by the European Organisation for Nuclear Research, CERN in Geneva [9]. The ROOT system is an object-oriented framework for large scale data handling. It is written in the C++ language. ROOT is very flexible and provides both a programming interface to use in its applications and a graphical user interface for interactive data analysis. ROOT provides a data structure, the tree, that is extremely powerful for fast access of huge amounts of data– orders of magnitude faster than accessing a normal file. Results can be displayed with histograms, scatter plots, and fitting functions. ROOT graphics may be adjusted in real-time by a few mouse clicks. Publication-quality figures can be saved in PDF or other formats. In the present analysis, we use the root 5.34 version.

2.4 Anisotropic flow in heavy-ion collisions

The main topic of this thesis is elliptic flow. It has the most dominant contribution to anisotropic flow, which was briefly introduced in the previous chapter. The elliptic flow will be treated in detail in this chapter.

A non-central heavy-ion collision is illustrated as shown in Fig. 2.3. It shows the two heavy-ions just after they have collided. In the middle, the reaction volume is elliptically shaped, while the spectators (particles outside the overlap area between the two nuclei) continue to move in the beam direction Z [10].

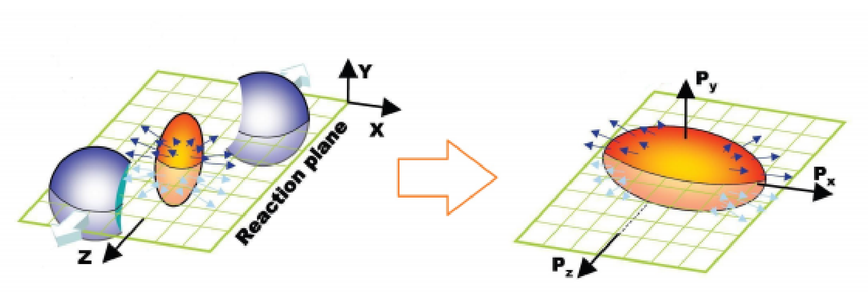

Figure 2.3: (Color online) Non-central heavy-ion collision with an elliptical reaction volume.

The spatial anisotropy of the overlap zone ensures the anisotropic pressure gradients in the transverse plane. This leads to a final state characterized by momentum anisotropy, an anisotropic azimuthal distribution of particles, and hence a non-vanishing v_n [11]. A convenient way of characterizing the various pattern of anisotropic flow is to use Fourier expansion of the momentum distribution with respect to the reaction plane angle Ψ_R,

$$E\frac{d^3N}{d^3p} = \frac{d^3N}{p_T dp dy d\phi}\frac{1}{2\pi}\left\{1 + \sum_{n=1}^{\infty} 2v_n \cos n(\phi - \psi_R)\right\}. \qquad (2.5)$$

Here E, p, p_{T} and y are the particle energy, momentum, transverse momentum, and rapidity respectively. ϕ is the azimuthal angle and v_n are the Fourier coefficients. Because of the symmetry with respect to the reaction plane, the sine terms in the expansion vanish and the Fourier coefficients can be calculated in the following way,

$$v_n(p_{\mathrm{T}}, y) =< \cos n(\phi - \psi_R) > \qquad (2.6)$$

The first harmonic v_1 represents an overall shift of the distribution in the transverse plane and is called directed flow. The second harmonic v_2 represents an elliptical volume and is called elliptic flow (v_2) [12]. The third harmonic gives a triangular flow and the fourth a squared flow. At mid -rapidity the second harmonic, elliptic flow (v_2) is dominant. For central collision the azimuthal distribution is isotropic, and hence $v_n = 0$, i.e only radial flow survives.

2.4.1 Elliptic flow

The first result of elliptic flow (v_2) proposed by the Relativistic heavy-ion Collider (RHIC) at Brookhaven National Laboratory indicated that the elliptical flow (v_2) approaches the prediction of a perfect liquid. The elliptic flow (v_2) is defined as the measure of the asymmetry of particle momentum distribution in the transverse plane and is generated by the anisotropic pressure gradient in the initial hot dense matter as a result of the spatial asymmetry in non-central (i.e. non -zero impact parameter (b)) collisions.

To acquire the high elliptic flow (v_2) in heavy-ion collisions, the shape of the interaction region should be asymmetric or almond-shaped, which depends on the impact parameter (b). The asymmetric shape is an important property for the generation of v_2. In the central collision, the value of impact parameter (b) is close to zero, produces low v_2 due to the symmetric shape of the interaction region. In peripheral collisions with a high value of impact parameter (b) results in an asymmetric interaction region but the interaction region is however small and thus also results in low v_2 [13]. Hence semi-central collisions produce maximum v_2 and the interacting particles in this asymmetric region provide a high value of pressure gradient along the minor axis which is along the x-axis and low-pressure gradient along the major axis which is along the y-axis. The fluid dynamic evolution of the produced QGP medium faces the anisotropic transverse gradient that converts the spatial anisotropy to momentum anisotropy, and hence a non-vanishing v_2.

Chapter 3

Results and Discussion

In heavy-ion collisions, symmetric nuclei such as Pb and Au are used to form the quark-gluon plasma. Experiments have been conducted at RHIC with uranium (U), which is heavier than Pb and Au ions and is considered to be highly deformed. Similarly at the LHC, this study has been carried out for Xe-nuclei (Xe being a deformed nucleus) [14]. A comparison of central collisions of spherical nuclei with those of deformed nuclei helps in establishing the fact that whether the elliptic flow observed in heavy-ion collisions is an initial state effect. Therefore, the collision of Xe-nuclei at $\sqrt{s_{NN}}$ = 5.44 TeV must be more interesting to study the hadronic phase time (τ_{HC}) dependence of elliptic flow (v_2) [15]. Using AMPT-SM model, we tried to study the effect of hadronic phase time (τ_{HC}) on identified particle production such as π, K, $\mathrm{K_s^0}$, p, ϕ and Λ in Xe+Xe collisions at $\sqrt{s_{\mathrm{NN}}}$ = 5.44 TeV. Finally, we study the transverse momentum (p_{T}) spectra and elliptic flow (v_2) of the identified particle at different τ_{HC} as a function of collision centrality.

3.1 p_{T}-Spectra of identified particles

The transverse momentum (p_{T}) spectra of identified particles in Xe+Xe collisions at $\sqrt{s_{NN}}$ = 5.44 TeV using AMPT-SM model is shown for (30-40)% centrality class in the top panel of Fig. 3.1 for different hadronic phase time. The bottom panel shows the ratio with respect to 25 fm. Different symbols represent the p_{T} spectra for various hadronic phase time.

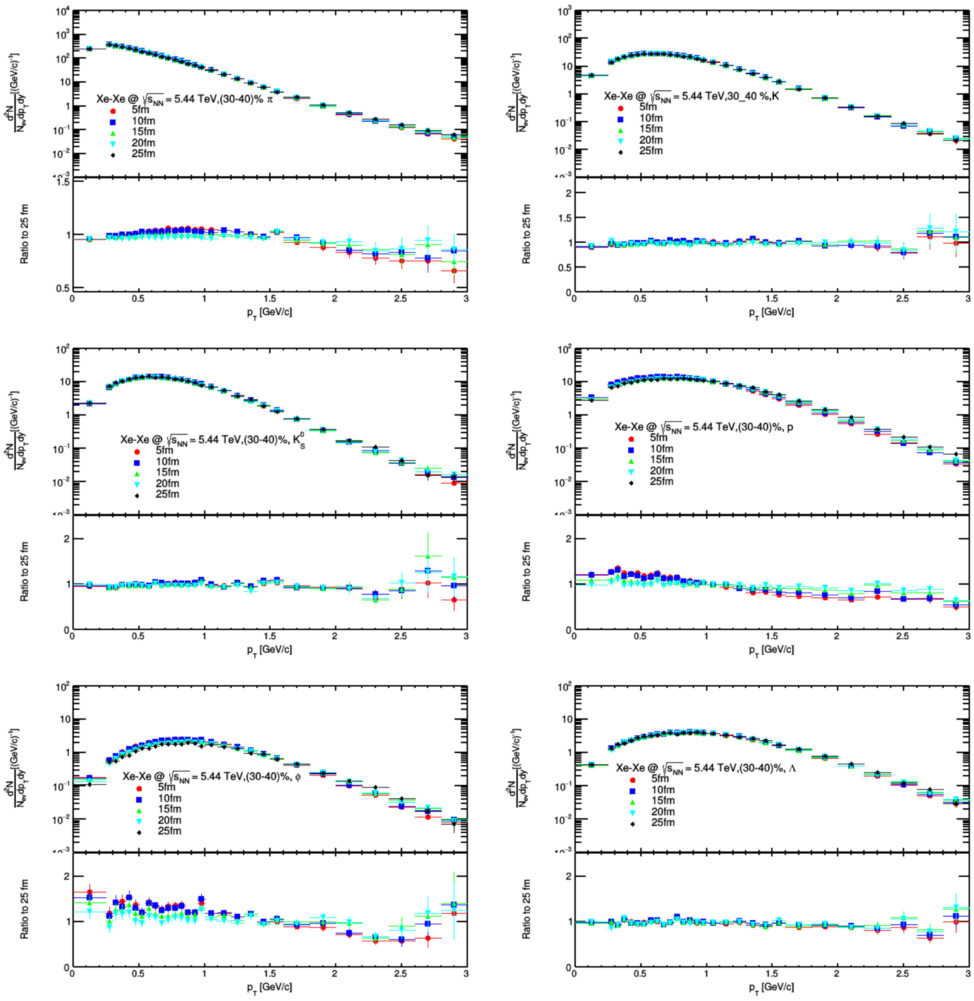

Figure 3.1: (Color online) Transverse momentum (p_{T}) spectra of identified particles in (30-40)% centrality class in Xe+Xe collisions at $\sqrt{s_{NN}} = 5.44$ TeV using AMPT model.

At low p_{T}, we observe a mass-dependent behavior of the produced particles. The hadron with light masses such as π, K are more produced in low p_{T} region than hadron with heavy masses such as ϕ and Λ. The peak of the transverse momentum spectra shifts towards the higher p_{T} due to the boost factor coming from the collectivity of the system produced in the heavy-ion collisions. This boost is higher for the heavier particles as shown from the transverse momentum spectra of identified particles. In Fig. 3.2, we have shown the p_{T} spectra of identified particles for (40-50)% centrality class. In appendix, we have shown the p_{T} spectra for most central collisions and peripheral collisions.

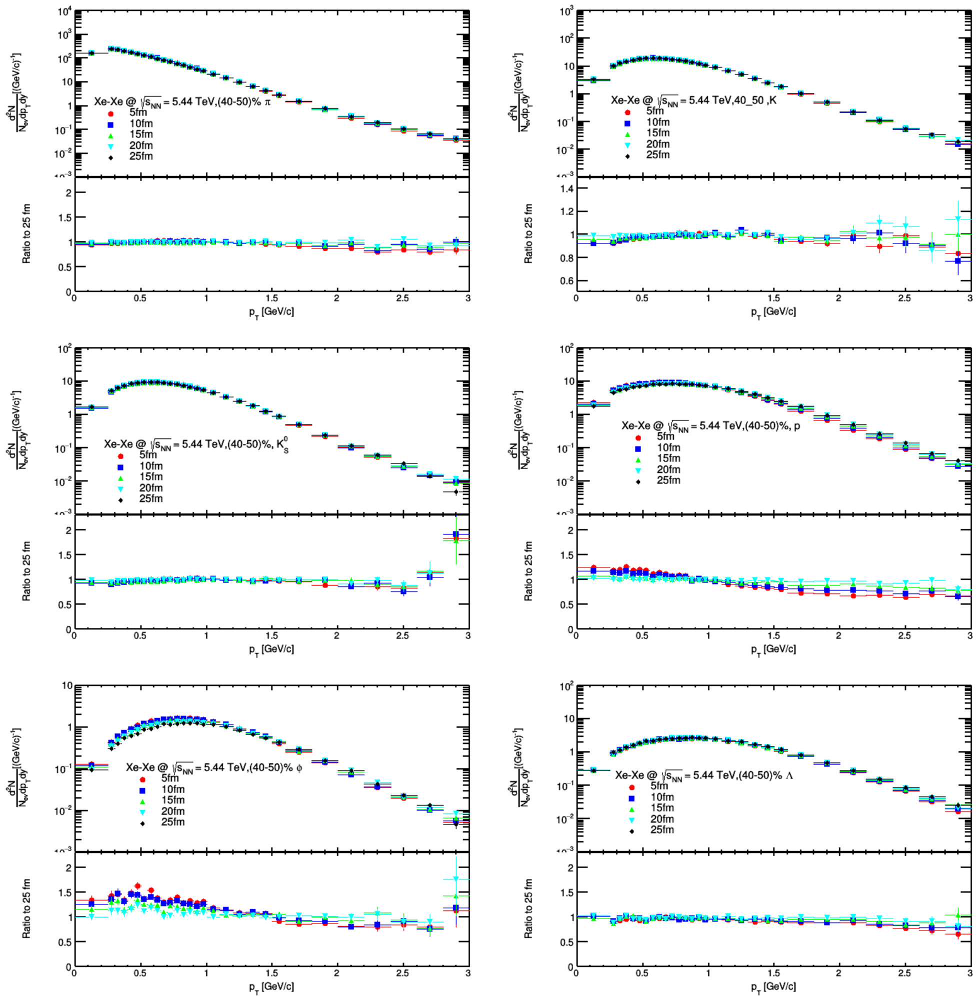

Figure 3.2: (Color online) Transverse momentum (p_{T}) spectra of identified particles in (40-50)% centrality class in Xe+Xe collisions at $\sqrt{s_{NN}} = 5.44$ TeV using AMPT model.

3.1.1 Minimum bias p_{T} -spectra (Decay: On)

In Fig 3.3, the transverse momentum (p_{T}) spectra of identified particles in Xe+Xe collisions at $\sqrt{s_{NN}} = 5.44$ TeV using AMPT-SM model are shown in the top panel for different hadronic phase time (τ_{HC}). The bottom panel shows the ratio with respect to 25 fm. Different symbols represent the p_{T} spectra for various hadronic phase time. If resonance particles such as $\mathrm{K}^0_{\mathrm{s}}$ ($\approx$ 4.16 fm/c) and ϕ ($\approx$ 46 fm/c) decay before the kinetic freeze-out then they are subjected to hadronic re-scattering of the daughter particles which will alter their momentum distributions. This has been demonstrated here by gradually increasing τ_{HC}, which allows a higher re-scattering effect. As

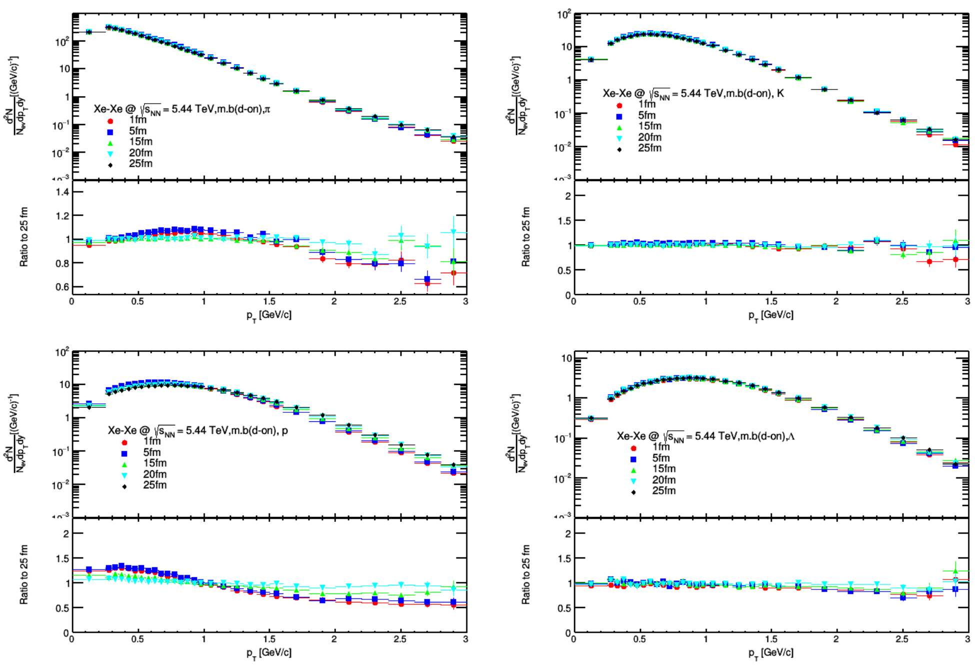

Figure 3.3: (Color online) Transverse momentum (p_{T}) spectra of π, K, p and Λ in Xe+Xe minimum bias collisions at $\sqrt{s_{NN}}$ = 5.44 TeV using AMPT model.

we allow the decay of $\mathrm{K}^0_{\mathrm{s}}$ and ϕ meson, it contributes to the final state π and K through the hadronic decay channels which have the largest branching ratios. We see a clear dependence of the hadronic phase lifetime on the transverse momentum spectra of the π and p as compared to the K. This results due to the higher interaction cross-section between π-π, π-p as compared to hadron-K interactions.

3.1.2 Minimum bias p_{T}-spectra (Decay: Off)

In Fig. 3.4 , we show p_{T} spectra of identified particles for minimum bias Xe+Xe collision at $\sqrt{s_{NN}}$ = 5.44 TeV using AMPT-SM model. The hadron decay off in this study doesn't allow $\mathrm{K}^0_{\mathrm{s}}$ and ϕ to decay through the hadronic channels. This reduces the number of the final state particles in the heavy-ion collisions. Hence the change in the hadronic cascade time does not affect the shape of the p_{T} spectra of all the identified particles except protons.

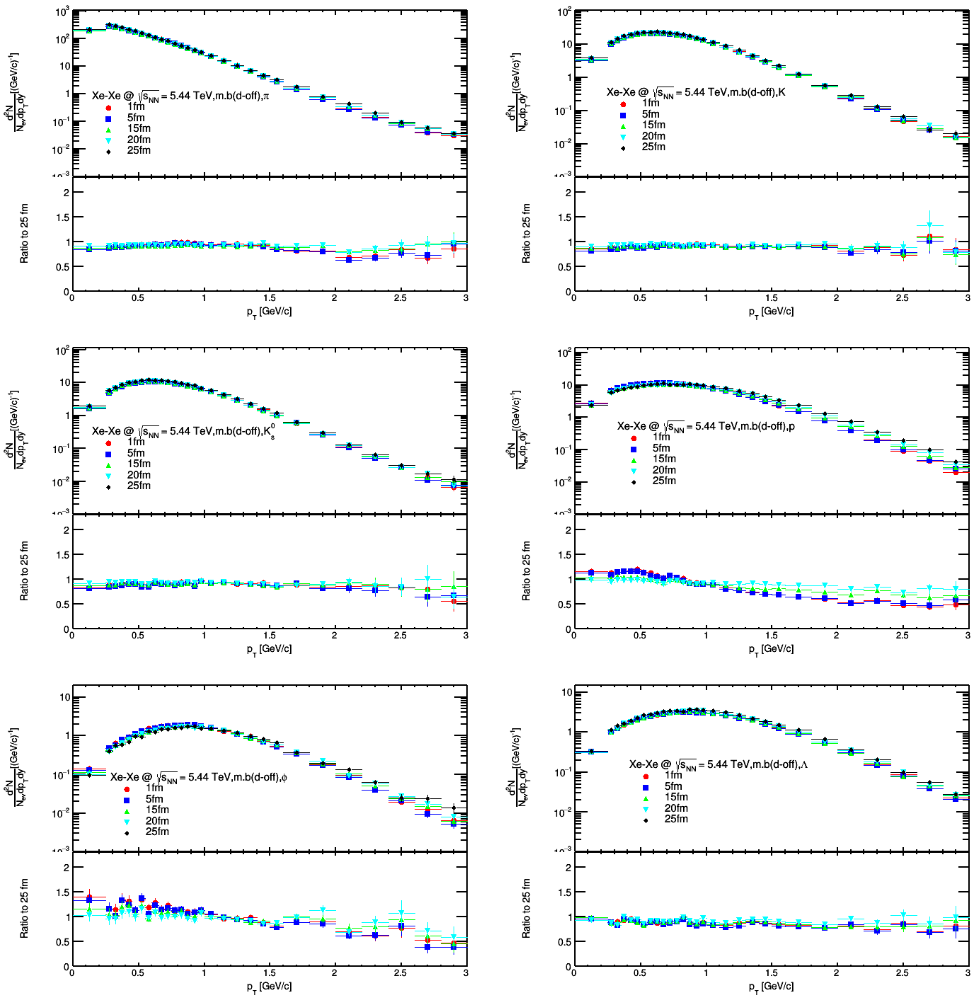

Figure 3.4: (Color online) Transverse momentum (p_{T}) spectra of identified particles in Xe+Xe minimum bias collisions at $\sqrt{s_{NN}}$ = 5.44 TeV using AMPT model.

3.2 Elliptic flow of identified particles

3.2.1 Minimum bias (Decay: On)

The p_{T} differential elliptic flow (v_2) for Xe+Xe minimum-bias collisions at $\sqrt{s_{NN}}$ = 5.44 TeV is shown in Fig. 3.5. Different symbols represent the elliptic flow (v_2) for various identified particles. A mass ordering of the elliptic flow (v_2) is observed at low transverse momentum region.

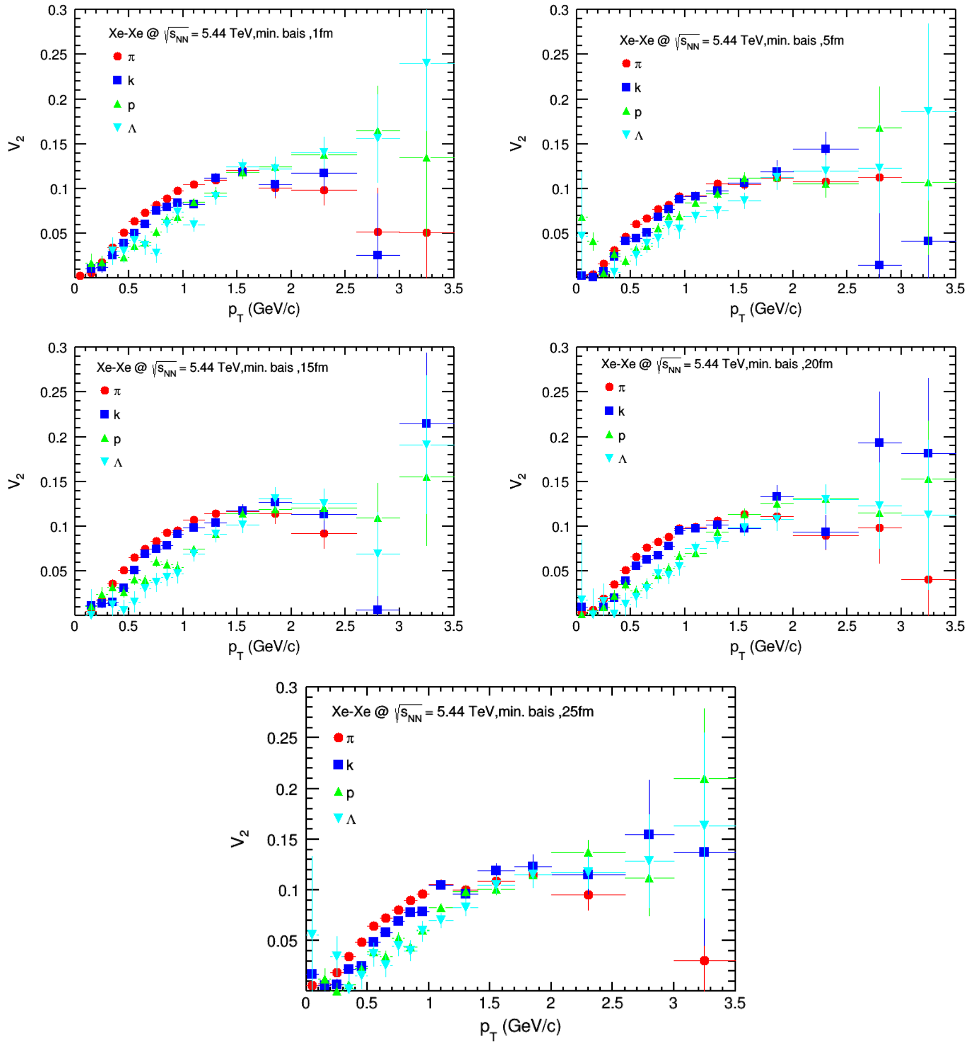

Figure 3.5: (Color online) Elliptic flow (v_2) of π, K, p and Λ in Xe+Xe minimum-bias collisions at $\sqrt{s_{NN}}$ = 5.44 TeV using AMPT-SM model.

3.2.2 Centrality dependence

Centrality dependence of elliptic flow (v_2) as a function of p_{T} for π in Xe+Xe collisions at $\sqrt{s_{NN}}$ = 5.44 TeV is shown in Fig. 3.6 for various hadronic phase time. The elliptic flow (v_2) is higher for the semi-peripheral collisions as the spatial anisotropy of the colliding nuclei is higher which results in the final state momentum anisotropy. In case of the most central and most peripheral collisions, the elliptic flow is lower. However, the physics origin in both cases is different. In most central collisions, the colliding region is not perfectly almond-shaped rather more spherical which results in less momentum anisotropy. Whereas in the ultra-peripheral collisions,

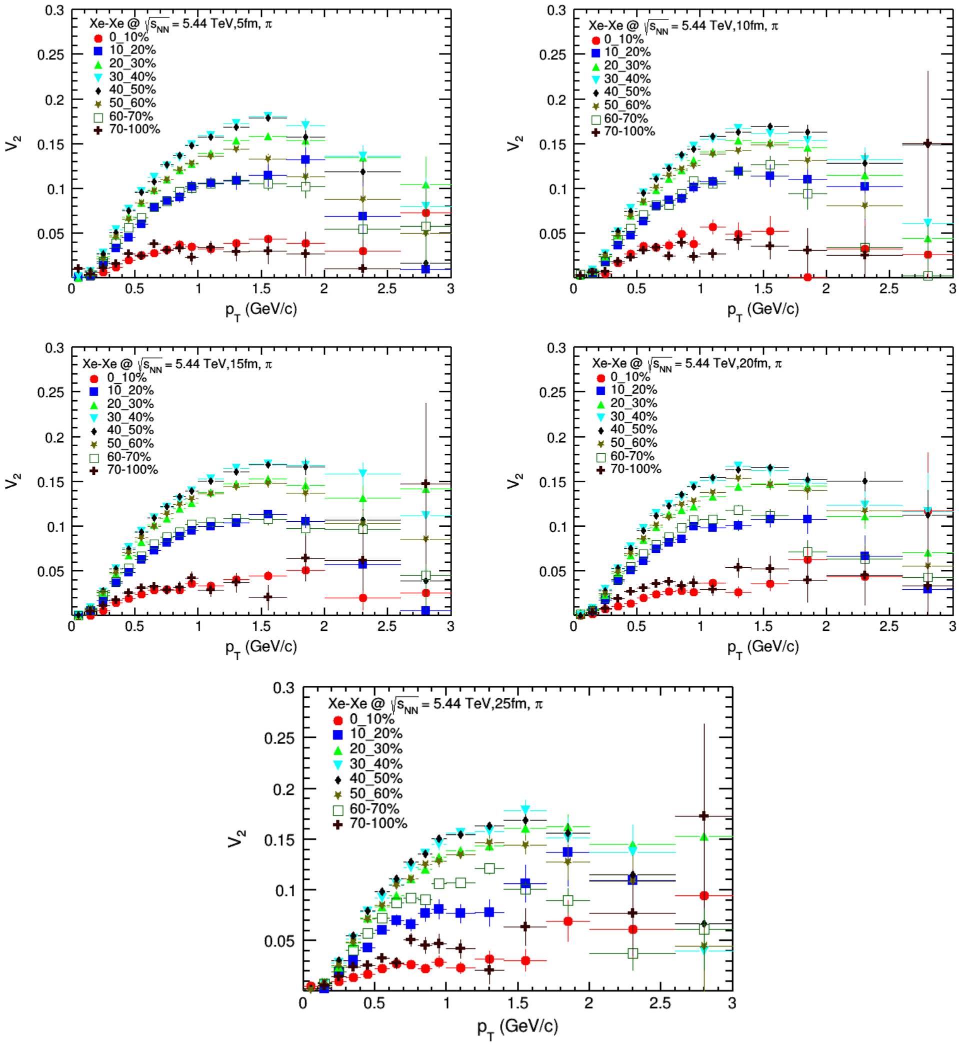

Figure 3.6: (Color online) Centrality dependence of elliptic flow (v_2) as a function of $p_{\rm T}$ for π in Xe+Xe collisions at $\sqrt{s_{NN}} = 5.44$ TeV using AMPT model.

the number of participants is very less resulting in the lower values of the anisotropic flow. In appendix, we have shown the v_2 vs $p_{\rm T}$ distribution for all other identified particles such as K, $\rm K^0_s$, p, ϕ and Λ in Xe+Xe collisions at $\sqrt{s_{\rm NN}} = 5.44$ TeV.

3.2.3 Average elliptic flow ($< v_2 >$) of charged particles

Average elliptic flow ($< v_2 >$) as a function of centrality for charged particles is shown in Fig. 3.7. As discussed earlier, the $< v_2 >$ increases from high to low centrality classes which then saturates and decreases for the most peripheral collisions. For central collisions, by allowing the final state particles to interact for the higher hadronic cascade time leads to more isotropic distributions of the transverse momentum resulting lower values of $< v_2 >$ compared to smaller hadronic cascade time. This trend becomes reverse as we move to semi-central collisions, where the initial state spatial anisotropy takes over and higher hadronic cascade time increase the $< v_2 >$ further.

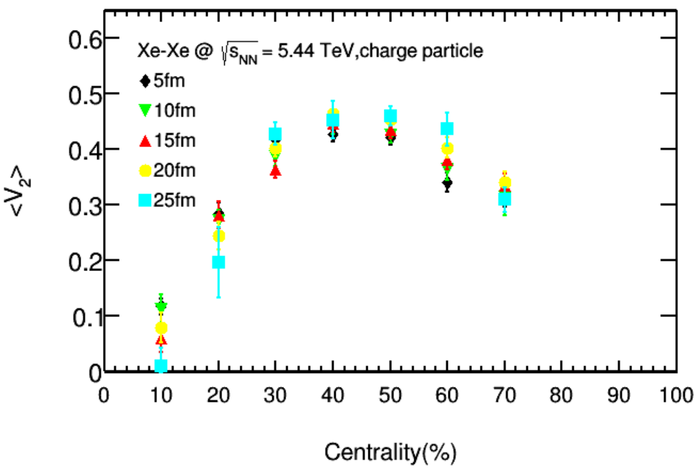

Figure 3.7: (Color online) Charged particles average elliptic flow ($< v_2 >$) with centrality in Xe+Xe collisions at $\sqrt{s_{NN}} = 5.44$ TeV using AMPT-SM model.

3.2.4 Baryon to meson elliptic flow ratio

Here we have tried to study the baryon (p) to meson (ϕ) elliptic flow ratio in different hadronic phase time (τ_{HC}) as they have similar masses. For this, in Fig. 3.8, we have shown the elliptic flow of p and ϕ in the upper panel and the v_2 ratio of p to ϕ in the bottom panel. Due to insufficient statistics, we are unable to bring up any conclusion regarding this Fig. 3.8. Later, we will try to look into baryon to meson elliptic flow ratio properly with sufficient statistics. In the appendix, we have shown the baryon (p) to meson (ϕ) elliptic flow ratio for different centrality classes.

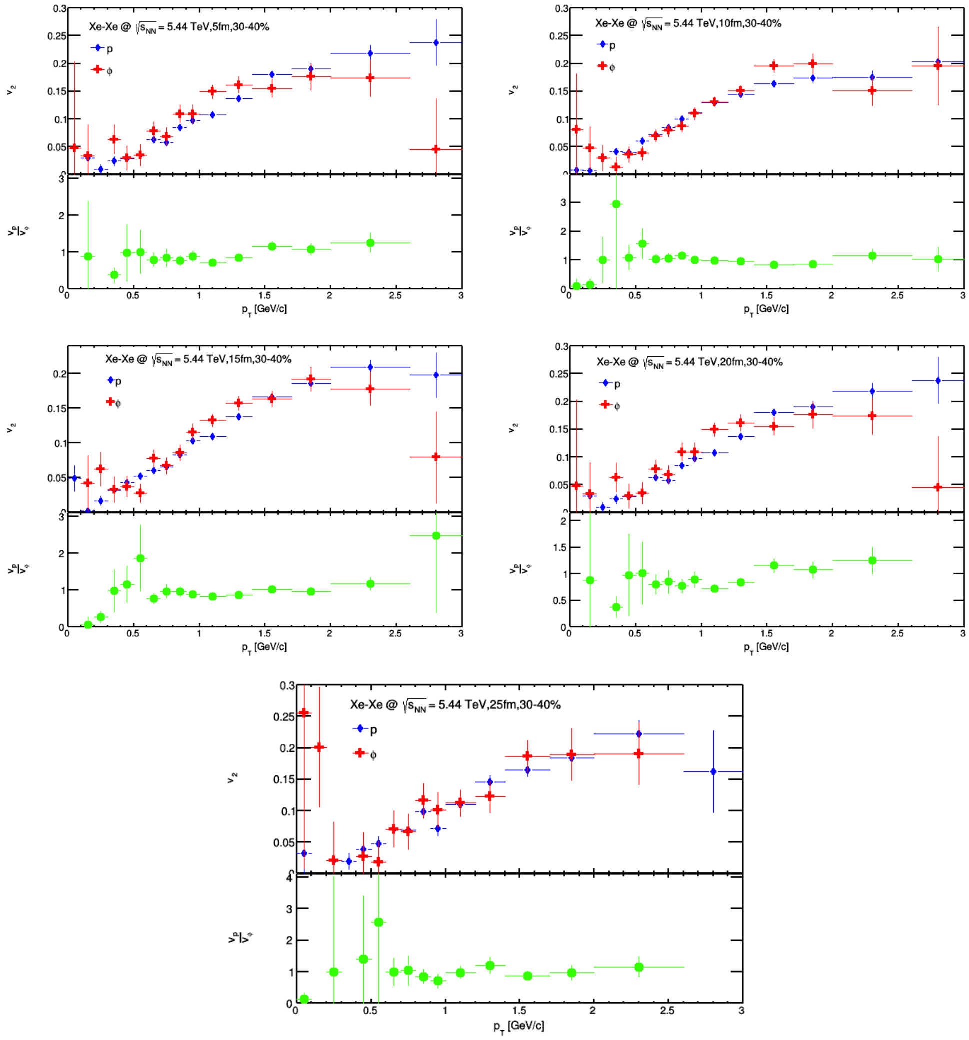

Figure 3.8: (Color online) Elliptic flow ratio of proton to phi for $(30-40)\%$ centrality class in $Xe+Xe$ collisions at $\sqrt{s_{NN}} = 5.44$ TeV for different τ_{HC} using AMPT model.

Chapter 4

Summary and Conclusions

To carry out the simulations of the heavy-ion collision, we have used A Multi-Phase Transport (AMPT) model. Here, we have studied the p_{T} spectra and elliptic flow (v_2) of both charged and identified particles in Xe+Xe collisions at $\sqrt{s_{NN}}$ = 5.44 TeV using AMPT-SM model. In the AMPT model, one can vary the termination time of the hadronic phase using a parameter - "NTMAX". Larger the hadronic phase time, more is the re-scattering among the decay particles. In this work, we have studied the p_{T} spectra of identified particles by varying the hadronic phase time (τ_{HC}), where we observe a mass-dependent behavior of the identified particles and also the shape depends on the τ_{HC}.

The most important observable in this study is the elliptic flow (v_2), which gives the experimental measurement of the momentum anisotropies produced in the heavy-ion collisions. The elliptic flow (v_2) as a function of p_{T} for different hadronic phase time (τ_{HC}) is obtained for various identified particles. The exposure of the fireball to large τ_{HC} values results in the higher re-scattering of the final state particles. In case of min. bias., at low p_{T} region the elliptic flow is less and then increases with p_{T} and finally saturates for high p_{T}. The non-zero value of v_2 confirms the presence of anisotropy in the collective flow of identified hadrons. The centrality dependence of v_2 as a function of p_{T} shows that v_2 increases with a decrease in centrality and it attains the maximum values for the mid-central collisions. This confirms the presence of a different degree of anisotropy for different centralities in heavy-ion collisions. The average elliptic flow ($\langle v_2 \rangle$) has lower values for the most-central collisions due to the lack of initial spatial-anisotropy of the colliding system. However, with decreasing centrality the initial spatial-anisotropy becomes larger and larger which gives rise to higher $\langle v_2 \rangle$. Moreover, this is not true in the case of most peripheral collisions as the number of participant nucleons is very less to generate collectivity in the produced system. The effect of different τ_{HC} on $\langle v_2 \rangle$ as a function of centrality classes in this work tells us about the generation of momentum anisotropy of final state particles form the life-time of the hadronic phase. For mid-central collisions, the $\langle v_2 \rangle$ is higher for the τ_{HC}= 25 fm/c, whereas an opposite behavior is observed for the central and the most peripheral classes. In future, the study of $\langle v_2 \rangle$ as a function of centrality classes will be carried out for different identified particles with full statistics. This will tell us the contribution of $\langle v_2 \rangle$ from the hadronic phase for different identified particles as they have different scattering cross-sections.

Bibliography

[1] F. Karsch, E. Laermann and A. Peikert, Nucl. Phys. B **605**, 579-599 (2001).

[2] S. Tiwari and C. Singh, Adv. High Energy Phys. **2013**, 805413 (2013).

[3] R. Sahoo, arXiv:1604.02651 [nucl-ex].

[4] C. Wong, "Introduction to high-energy heavy ion collisions".

[5] J. Adam *et al.* [ALICE], Nature Phys. **13**, 535-539 (2017).

[6] Z. W. Lin, C. M. Ko, B. A. Li, B. Zhang and S. Pal, Phys. Rev. C **72**, 064901 (2005).

[7] R. Rath, S. Tripathy, R. Sahoo, S. De and M. Younus, Phys. Rev. C **99**, 064903 (2019).

[8] K. Nayak, S. Singha, M. Nasim and B. Mohanty, DAE Symp. Nucl. Phys. **62**, 962-963 (2017).

[9] R. Brun and F. Rademakers, Nucl. Instrum. Meth. A **389**, 81-86 (1997).

[10] R. S. Bhalerao, arXiv:1404.3294 [nucl-th].

[11] S. Chatrchyan *et al.* [CMS], Phys. Rev. C **87**, 014902 (2013).

[12] S. Singha and M. Nasim, Phys. Rev. C **93**, 034908 (2016).

[13] R. Snellings, New J. Phys. **13**, 055008 (2011).

[14] S. Acharya *et al.* [ALICE], Phys. Lett. B **788**, 166-179 (2019).

[15] S. Tripathy, S. De, M. Younus and R. Sahoo, Phys. Rev. C **98**, 064904 (2018).

Chapter 5

Appendix

5.1 p_{T} -Spectra

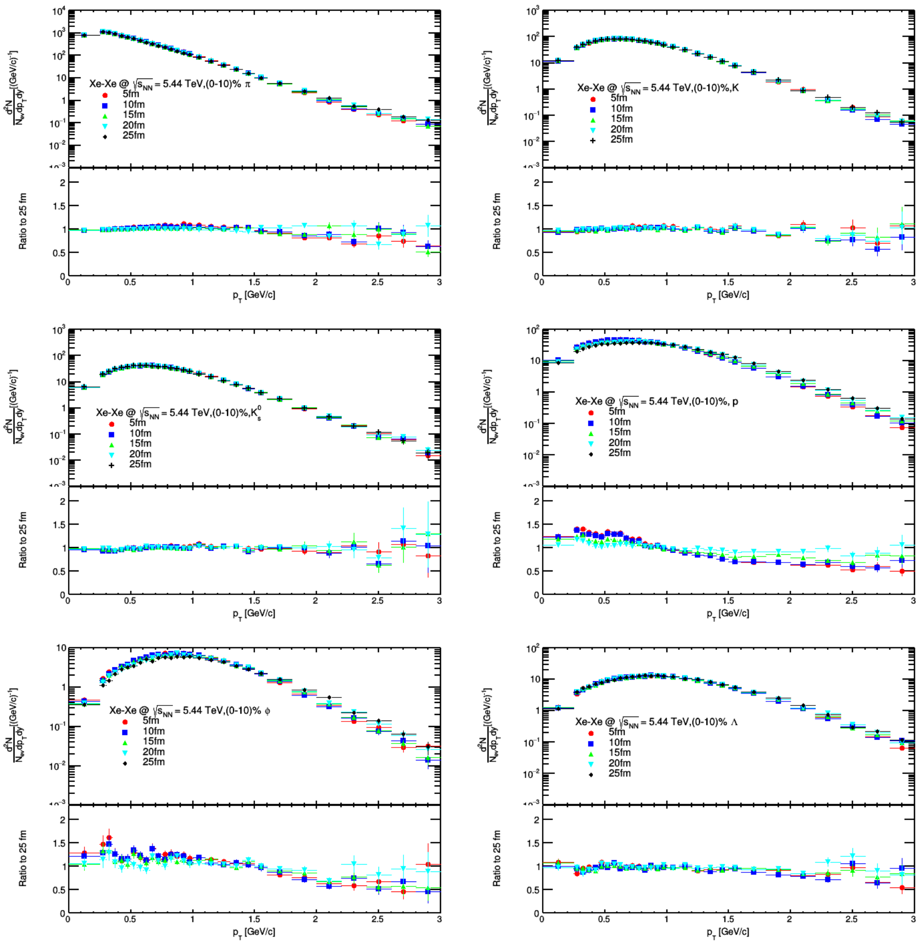

Figure 5.1: (Color online) Transverse momentum (p_{T}) distribution of identified particles in (0 -10)% centrality class in Xe+Xe collisions at $\sqrt{s_{NN}} =$ 5.44 TeV using AMPT model.

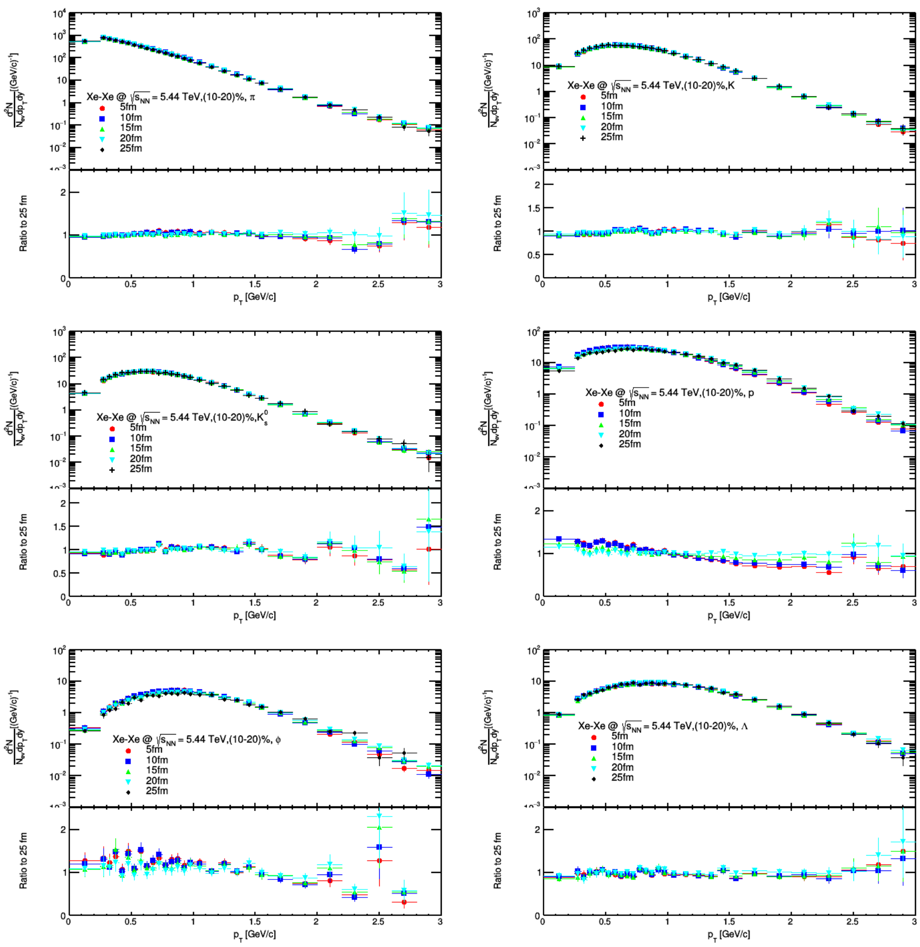

Figure 5.2: (Color online) Transverse momentum (p_{T}) distribution of identified particles in (10 -20)% centrality class in Xe+Xe collisions at $\sqrt{s_{NN}}$ = 5.44 TeV using AMPT model.

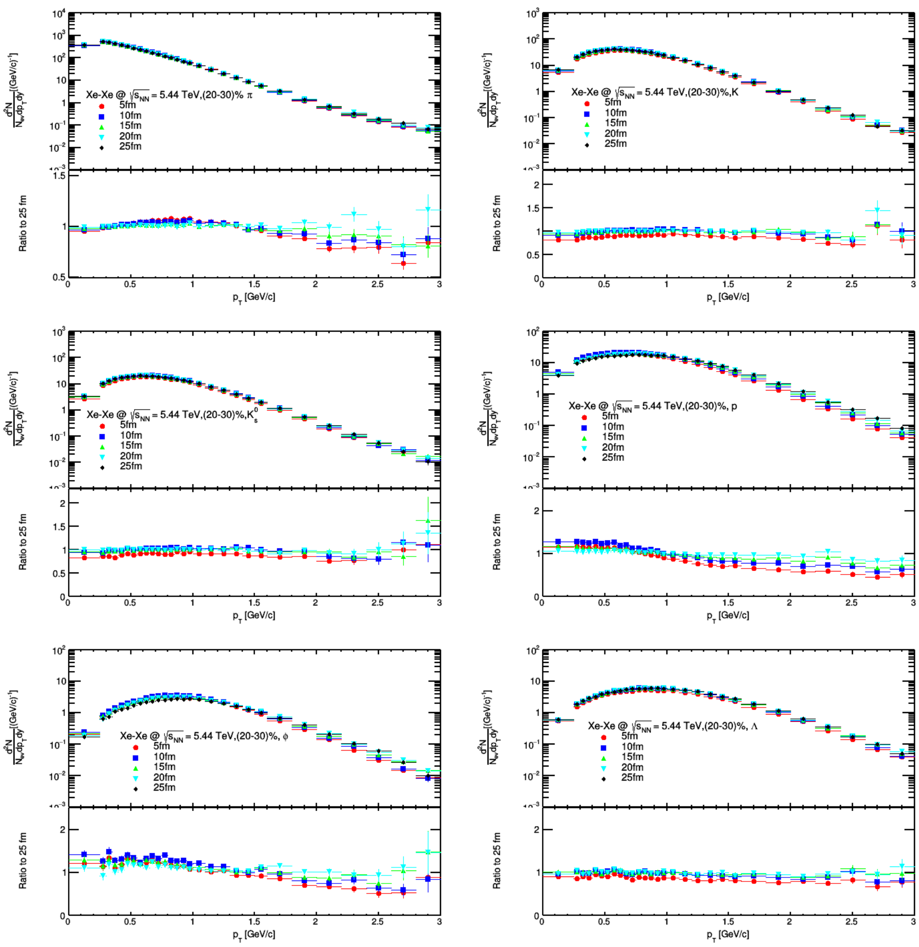

Figure 5.3: (Color online) Transverse momentum distribution (p_{T}) of identified particles in (20 -30)% centrality class in Xe+Xe collisions at $\sqrt{s_{NN}}$ = 5.44 TeV using AMPT model.

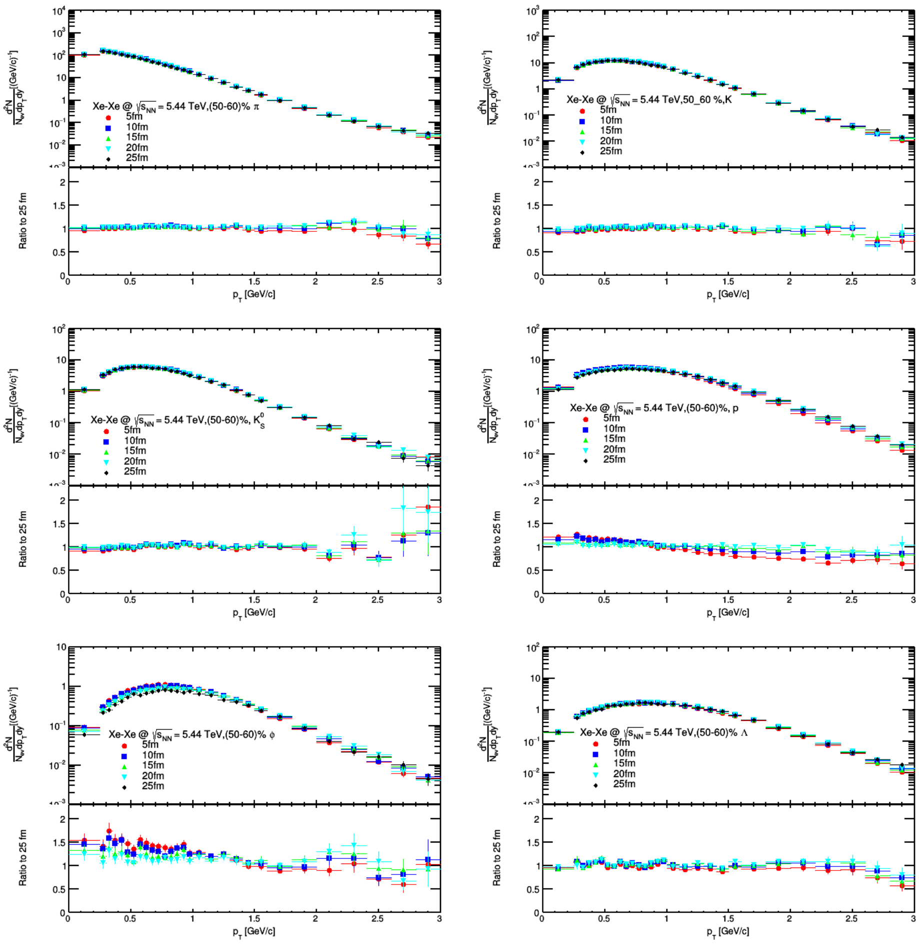

Figure 5.4: (Color online) Transverse momentum distribution ($p_{\rm T}$) of identified particles in (50 -60)% centrality class in Xe+Xe collisions at $\sqrt{s_{NN}}$ = 5.44 TeV using AMPT model.

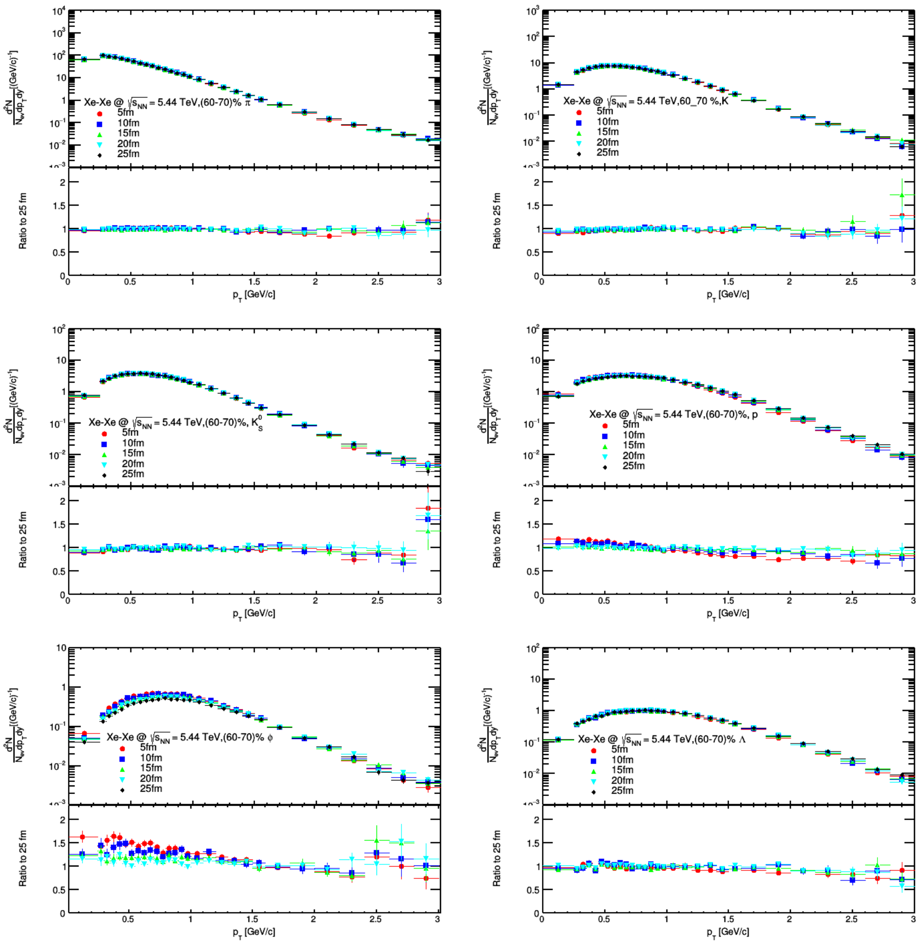

Figure 5.5: (Color online) Transverse momentum (p_{T}) distribution of identified particles in (60 -70)% centrality class in Xe+Xe collisions at $\sqrt{s_{NN}}$ = 5.44 TeV using AMPT model.

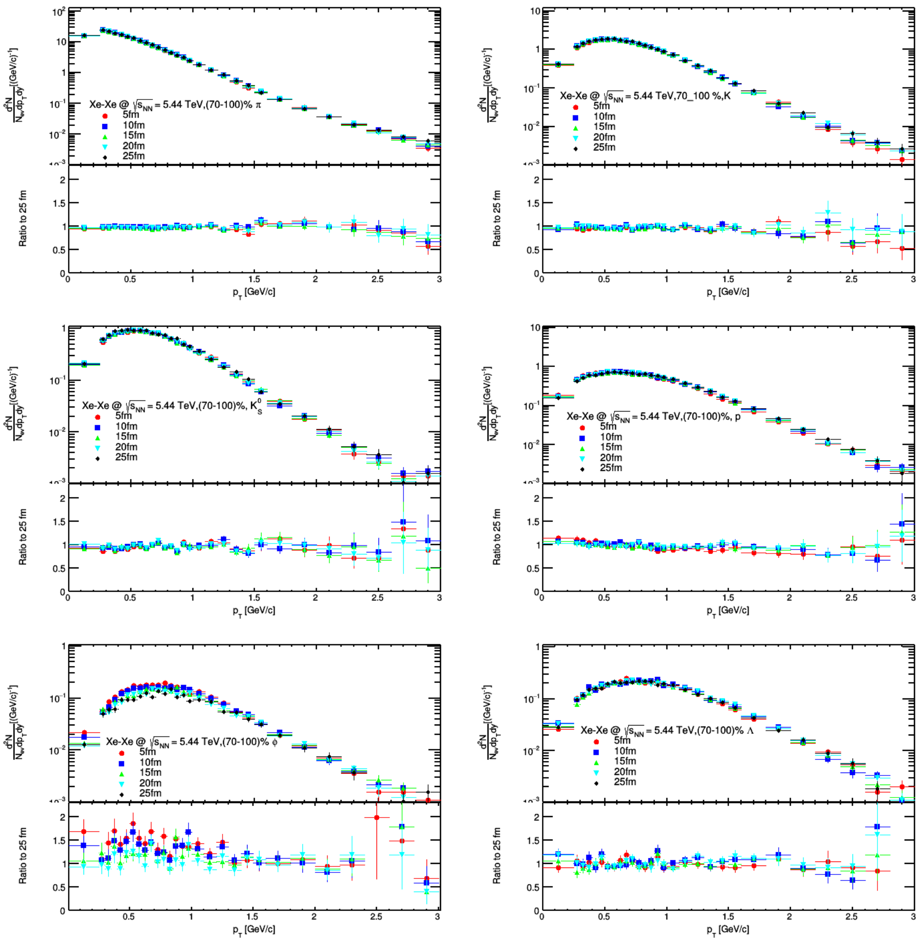

Figure 5.6: (Color online) Transverse momentum (p_{T}) distribution of identified particles in (70 -100)% centrality class in Xe+Xe collisions at $\sqrt{s_{NN}}$ = 5.44 TeV using AMPT model.

5.2 Elliptic Flow

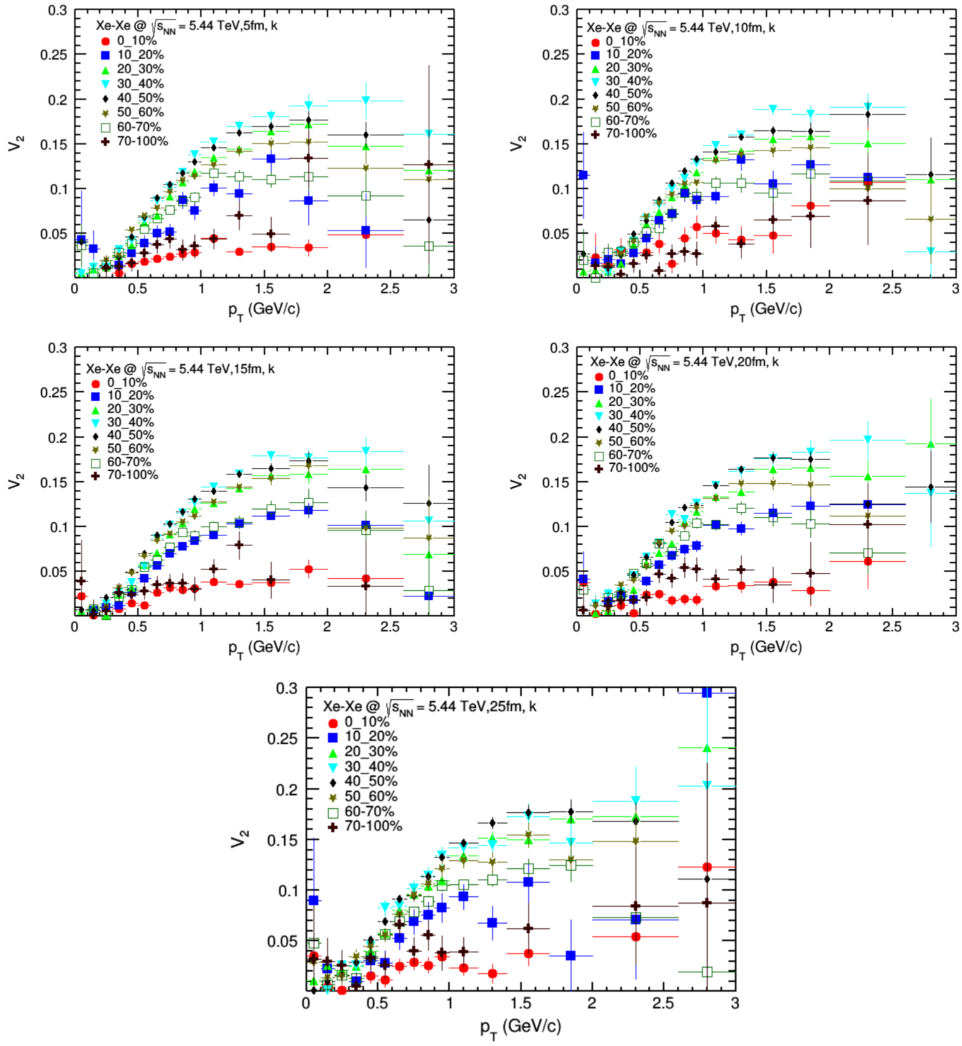

Figure 5.7: (Color online) Elliptic flow (v_2) of K in Xe+Xe collisions at $\sqrt{s_{NN}}$ = 5.44 TeV using AMPT-SM model.

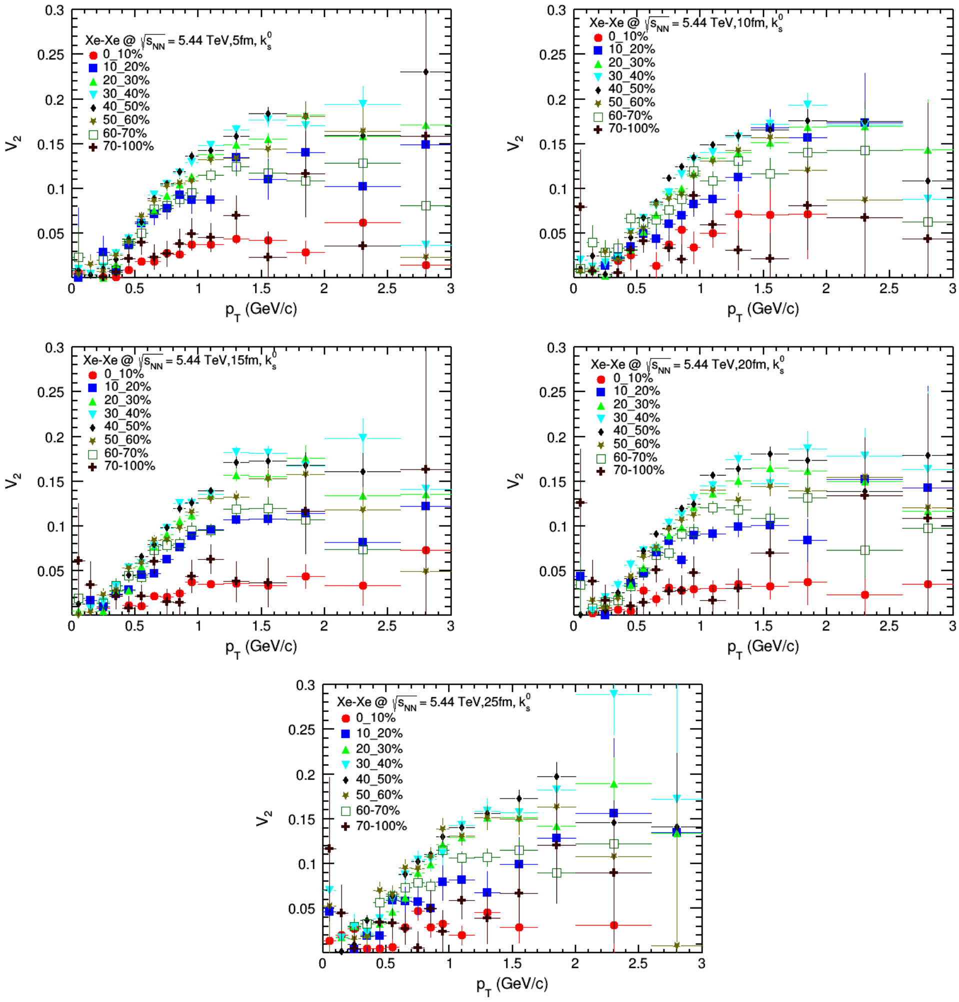

Figure 5.8: (Color online) Elliptic flow (v_2) of K_s^0 in Xe+Xe collisions at $\sqrt{s_{NN}} = 5.44$ TeV using AMPT-SM model.

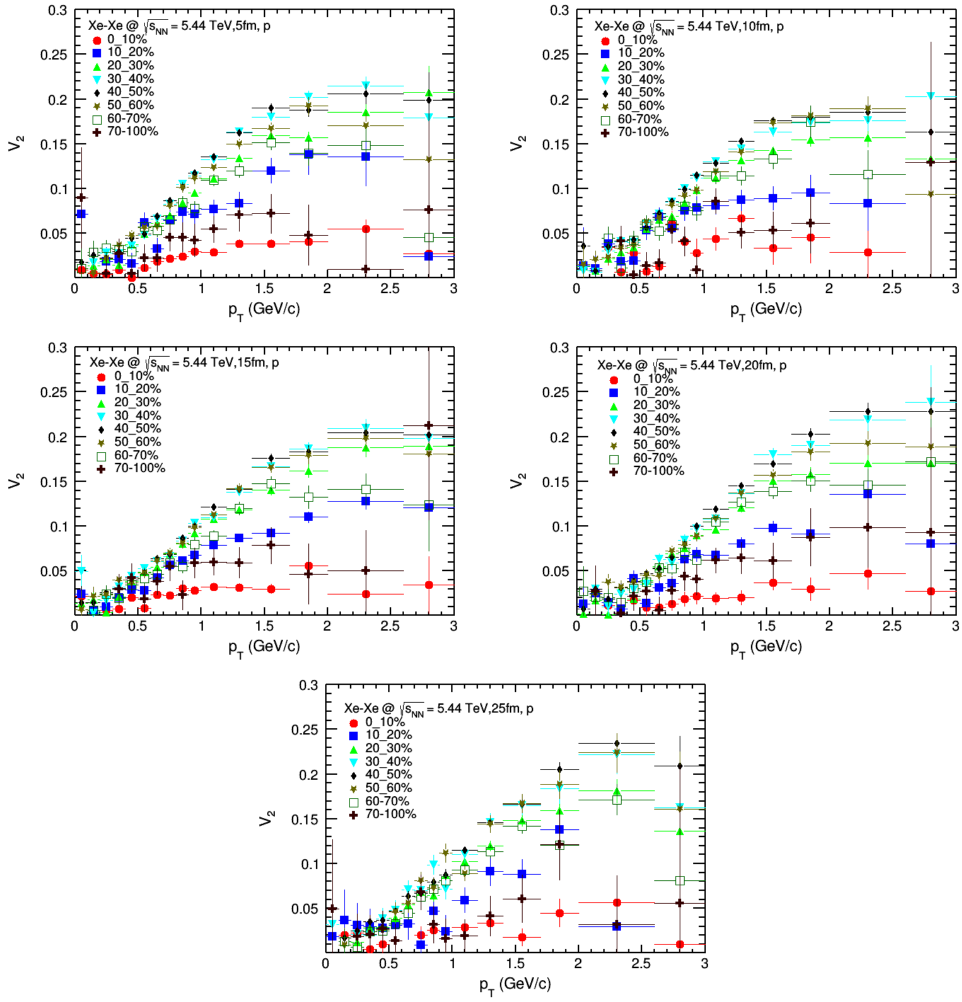

Figure 5.9: (Color online) Elliptic flow (v_2) of p in Xe+Xe collisions at $\sqrt{s_{NN}}$ = 5.44 TeV using AMPT-SM model.

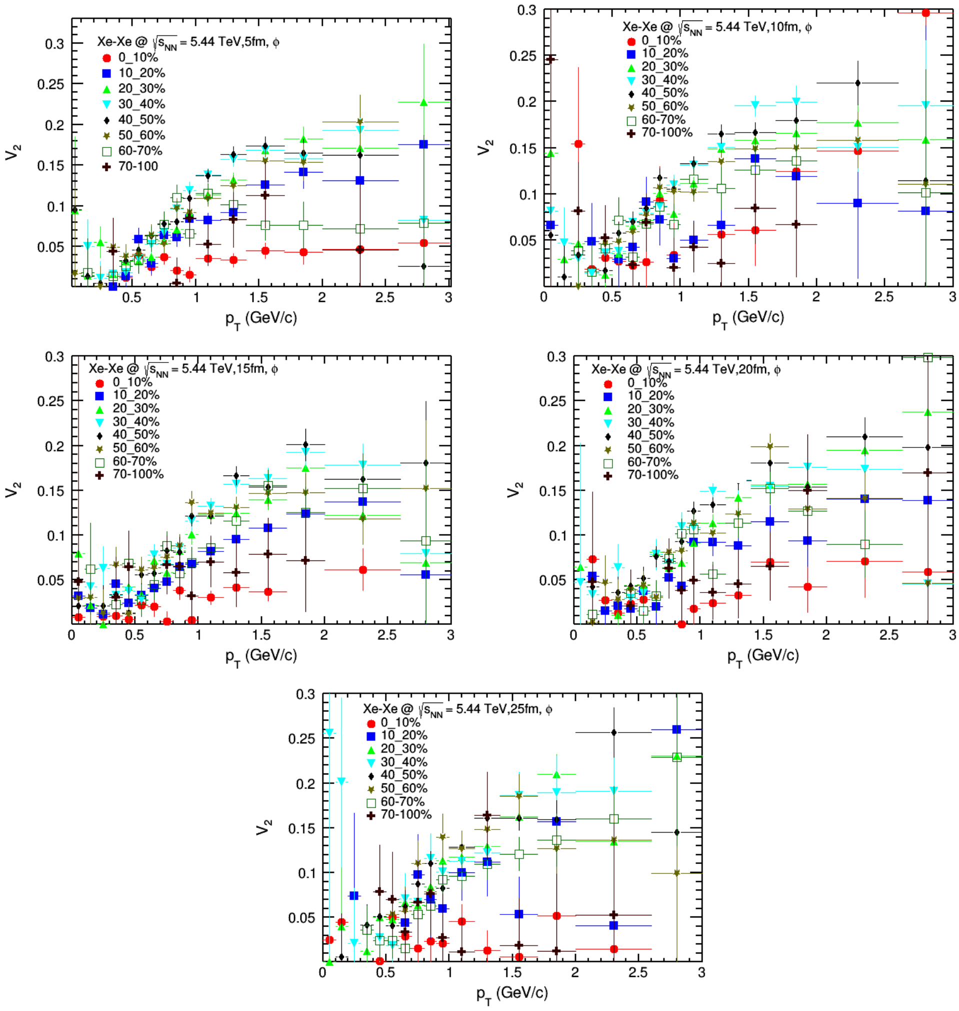

Figure 5.10: (Color online) Elliptic flow (v_2) of ϕ in Xe+Xe collisions at $\sqrt{s_{NN}} = 5.44$ TeV using AMPT-SM model.

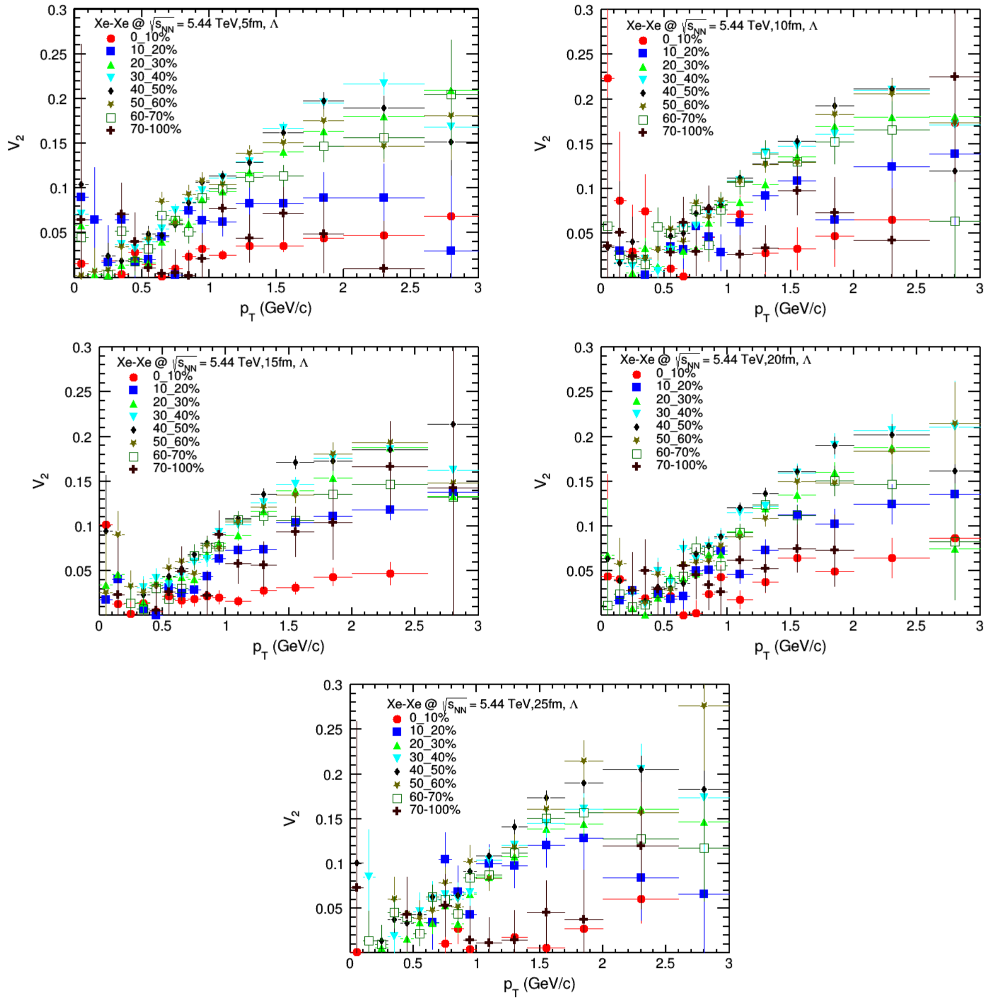

Figure 5.11: (Color online) Elliptic flow (v_2) of Λ in Xe+Xe collisions at $\sqrt{s_{NN}}$ = 5.44 TeV using AMPT-SM model.

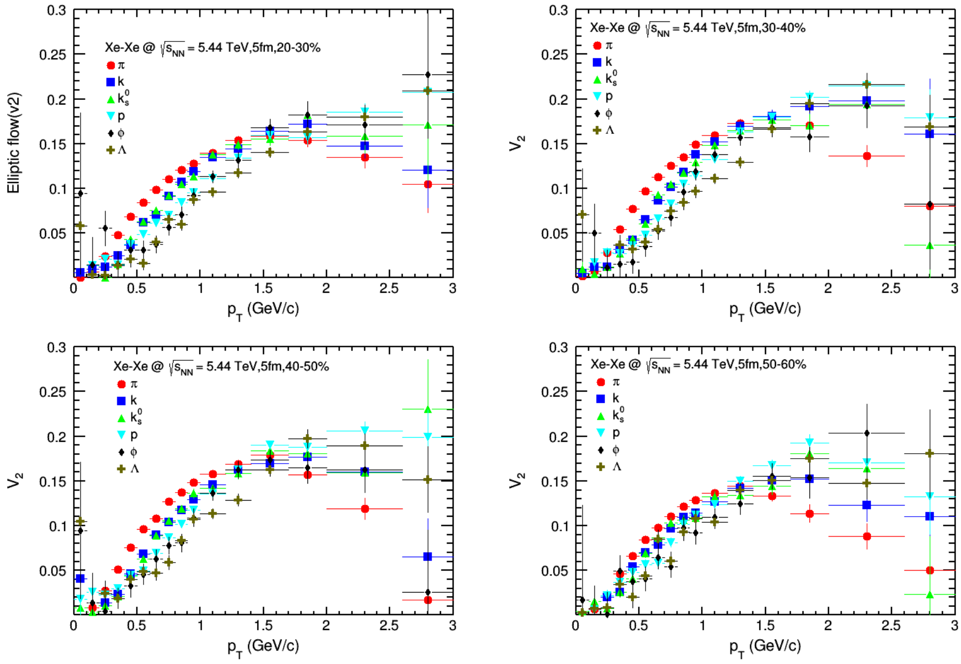

Figure 5.12: (Color online) Elliptic flow vs p_{T} distribution of identified particles for 5 fm in Xe+Xe collisions at $\sqrt{s_{NN}}$ = 5.44 TeV using AMPT-SM model.

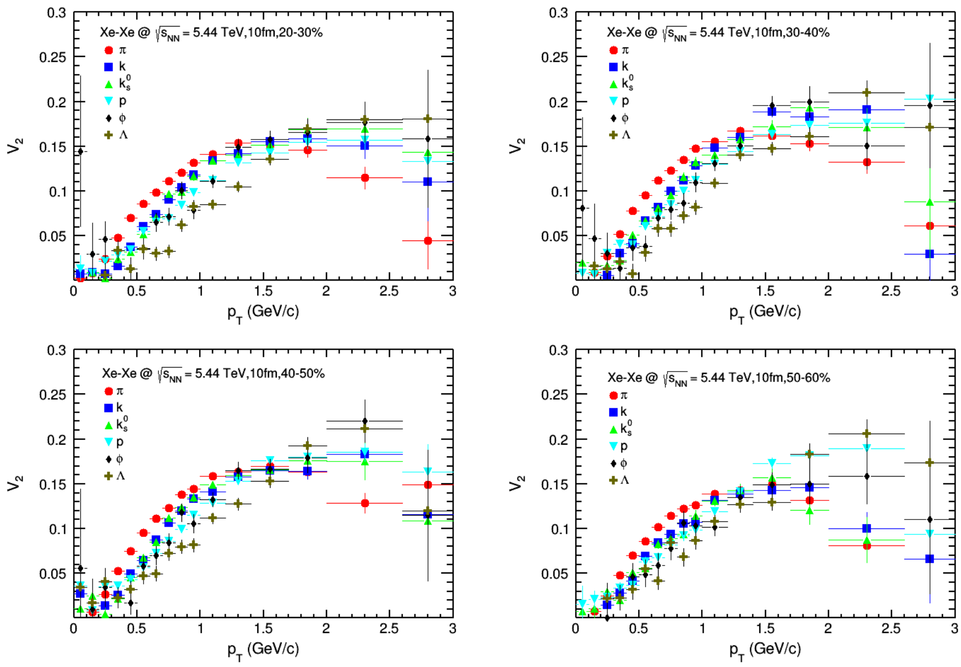

Figure 5.13: (Color online) Elliptic flow vs p_{T} distribution of identified particles for 10 fm in Xe+Xe collisions at $\sqrt{s_{NN}}$ = 5.44 TeV using AMPT-SM model.

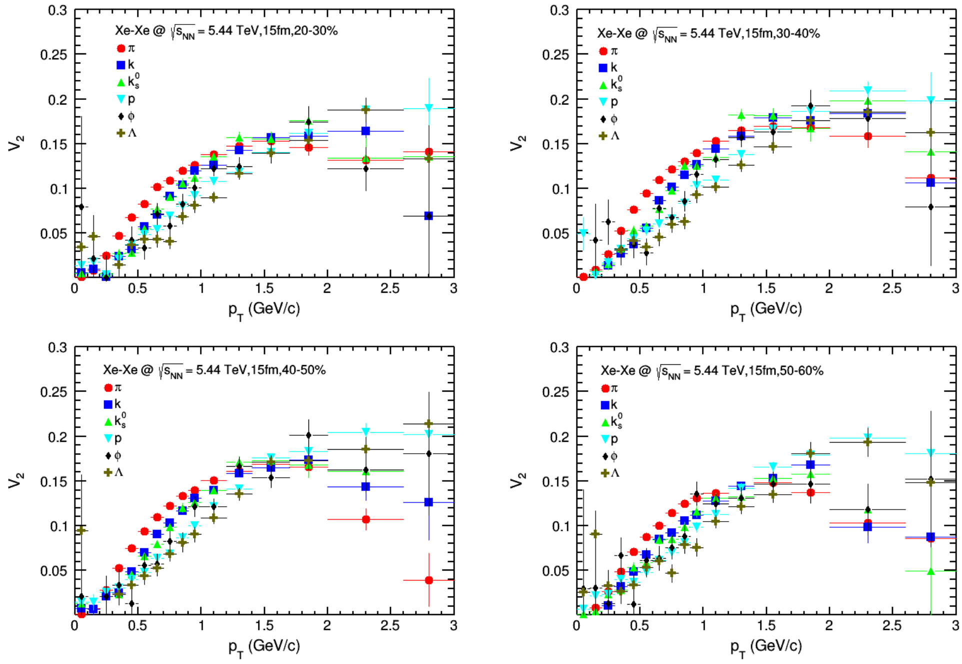

Figure 5.14: (Color online) Elliptic flow vs p_T distribution of identified particles for 15 fm in Xe+Xe collisions at $\sqrt{s_{NN}}$ = 5.44 TeV using AMPT-SM model.

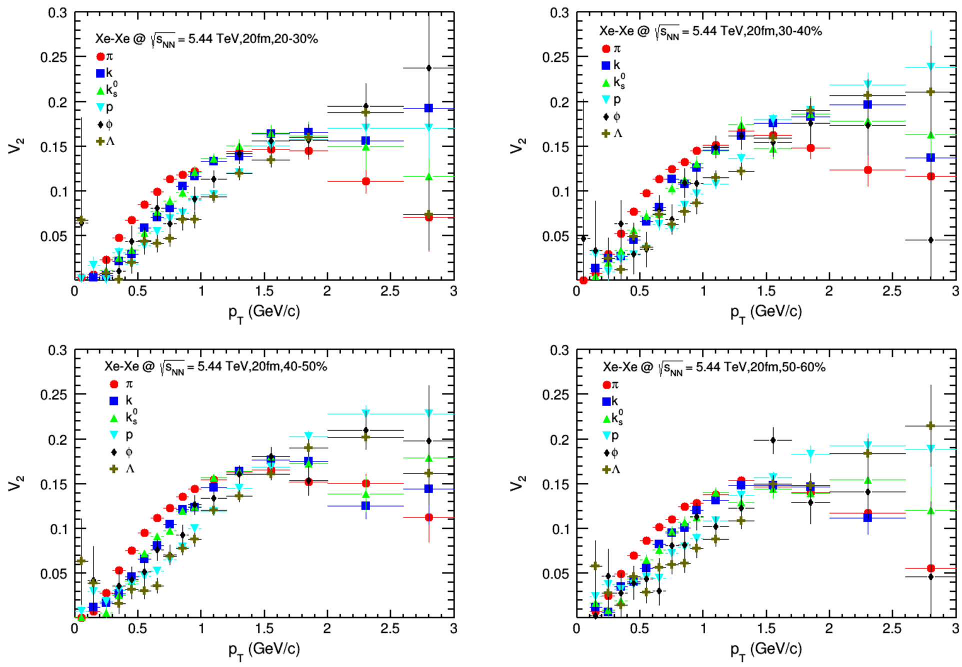

Figure 5.15: (Color online) Elliptic flow vs p_T distribution of identified particles for 20 fm in Xe+Xe collisions at $\sqrt{s_{NN}}$ = 5.44 TeV using AMPT-SM model.

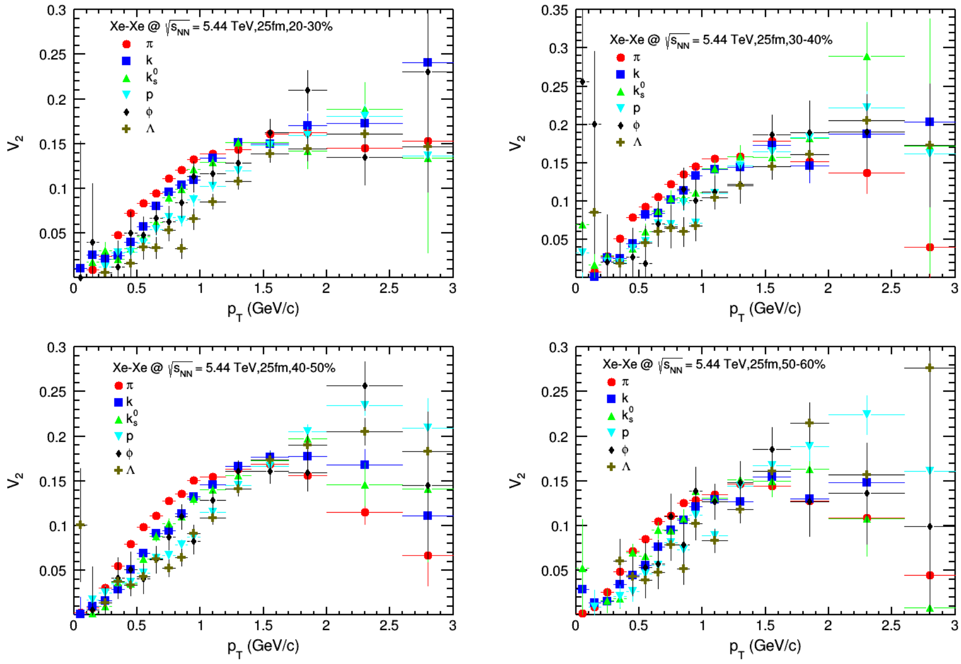

Figure 5.16: (Color online) Elliptic flow vs p_{T} distribution of identified particles for 25 fm in Xe+Xe collisions at $\sqrt{s_{NN}} = 5.44$ TeV using AMPT-SM model.

5.3 Baryon to Meson Ratio of Elliptic Flow

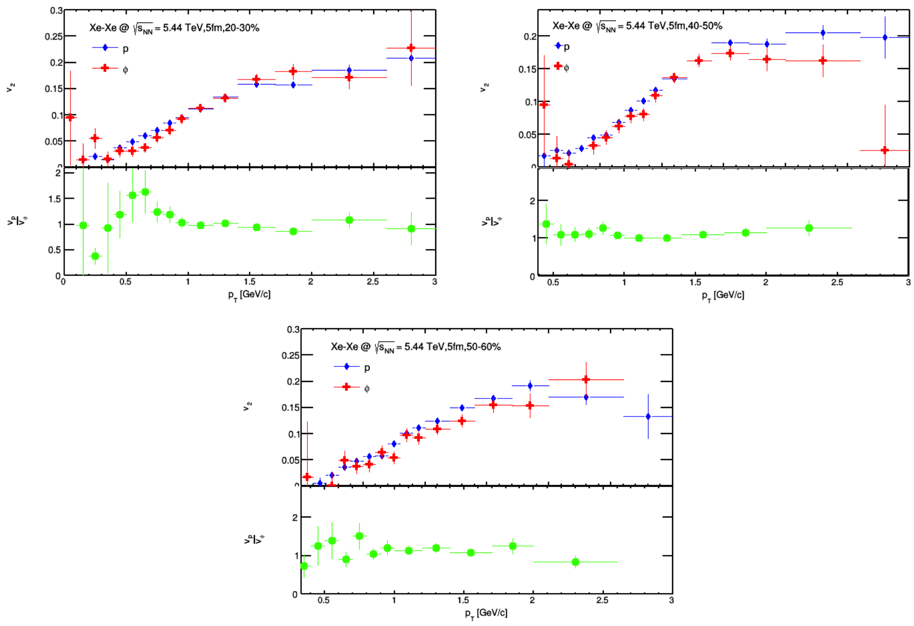

Figure 5.17: (Color online) Elliptic flow ratio of proton to phi for $\tau_{HC} =$ 5 fm in $Xe + Xe$ collisions at $\sqrt{s_{NN}} = 5.44$ TeV for different centrality classes using AMPT model.

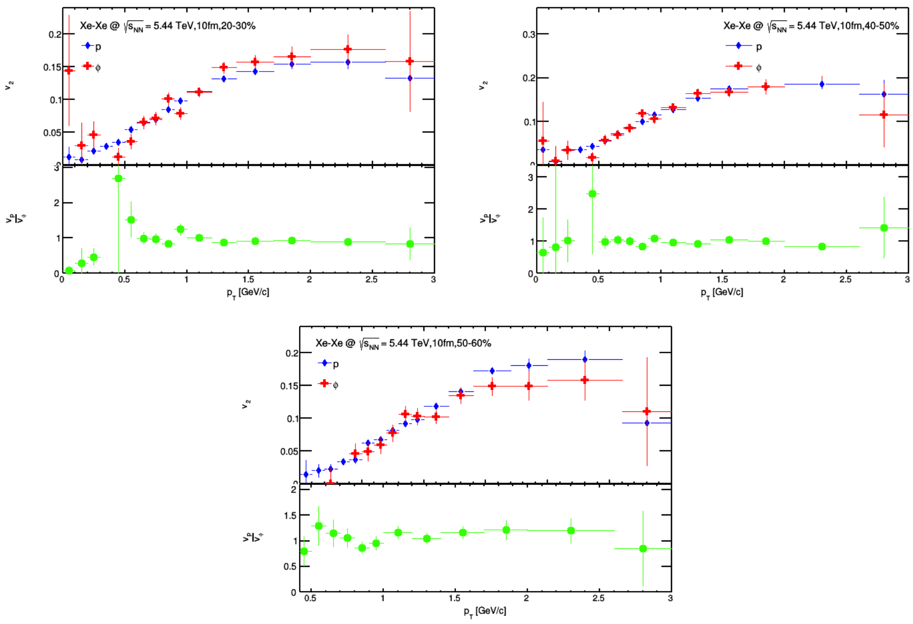

Figure 5.18: (Color online) Elliptic flow ratio of proton to phi for τ_{HC} = 10 fm in $Xe + Xe$ collisions at $\sqrt{s_{NN}}$ = 5.44 TeV for different centrality classes using AMPT model.

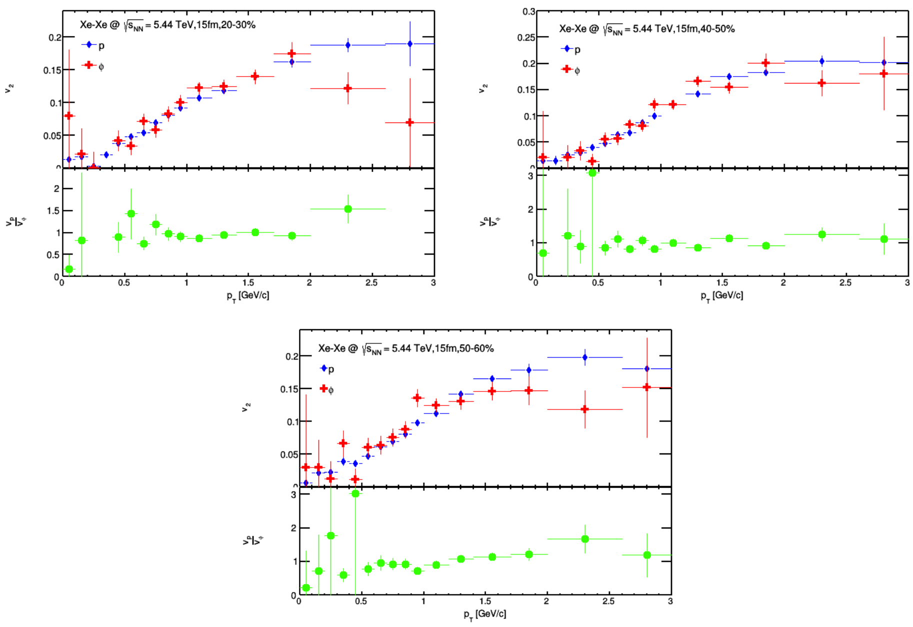

Figure 5.19: (Color online) Elliptic flow ratio of proton to phi for τ_{HC} = 15 fm in $Xe + Xe$ collisions at $\sqrt{s_{NN}}$ = 5.44 TeV for different centrality classes using AMPT model.

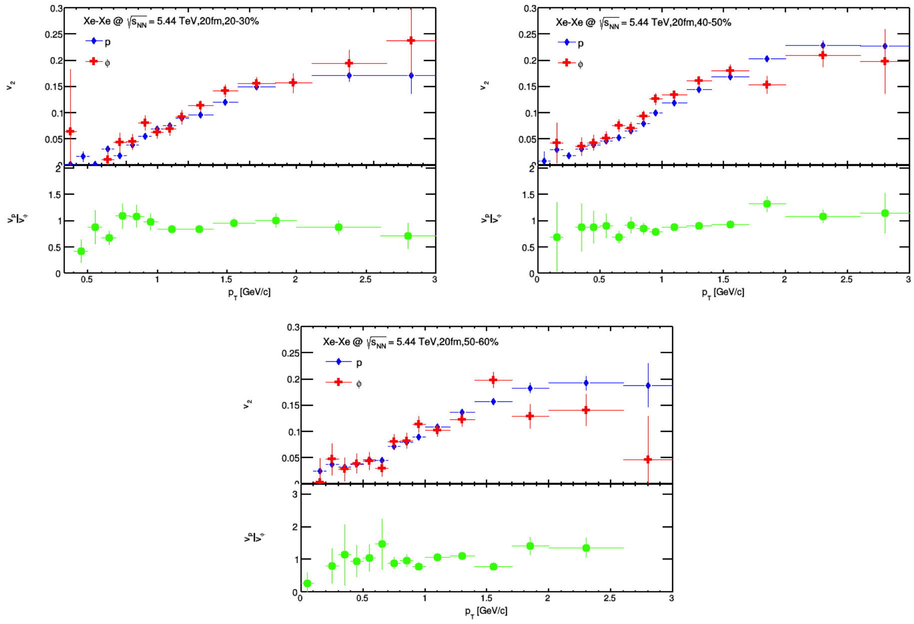

Figure 5.20: (Color online) Elliptic flow ratio of proton to phi for τ_{HC} = 20 fm in $Xe + Xe$ collisions at $\sqrt{s_{NN}}$ = 5.44 TeV for different centrality classes using AMPT model.

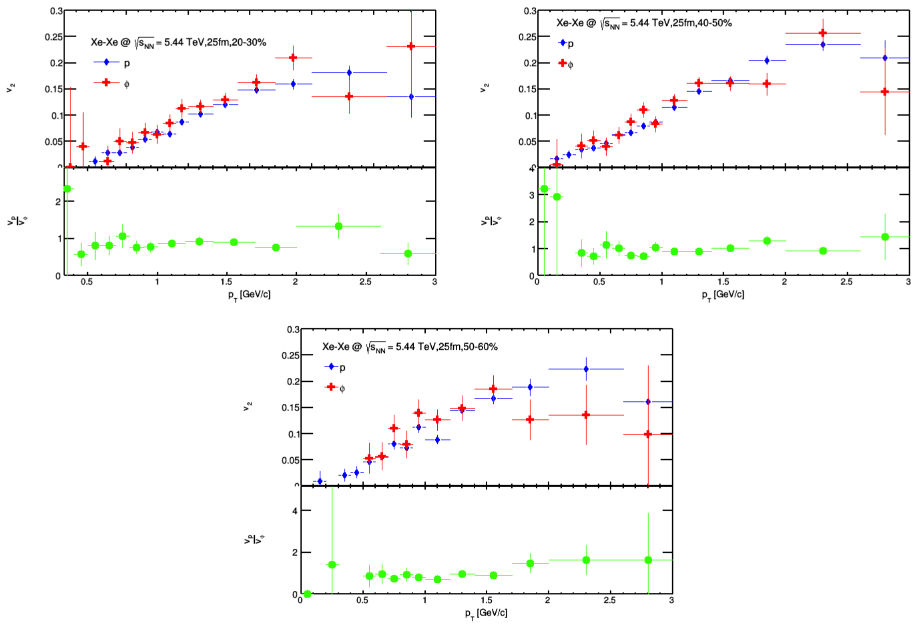

Figure 5.21: (Color online) Elliptic flow ratio of proton to phi for τ_{HC} = 25 fm in $Xe + Xe$ collisions at $\sqrt{s_{NN}}$ = 5.44 TeV for different centrality classes using AMPT model.